Preservation of contrasting geothermal gradients across the Caribbean-North America plate boundary (Motagua Fault, Guatemala)

T. Simon-Labric, G. Y. Brocard, C. Teyssier, P.A. van Der Beek, M.G. Fellin, P.W. Reiners, Christine Authemayou

Preservation of contrasting geothermal gradients across the Caribbean-North America plate boundary (Motagua Fault, Guatemala)

Thibaud Simon-Labric,[1] Gilles Y. Brocard,[2] Christian Teyssier,[3] Peter A. van der Beek,[1] Maria Giuditta Fellin,[4] Peter W. Reiners,[5] and Christine Authemayou[6]

[1]   Strike-slip plate boundaries juxtapose crustal blocks that may have different geodynamic origins and therefore different thermal structures. Thermo-kinematic modeling of this type of strike-slip plate boundary predicts an asymmetric signature in the low-temperature thermochronologic record across the fault. Age-elevation profiles of zircon (U-Th)/He ages across the Motagua Fault, a 500 km long segment of the transform boundary between the North American and Caribbean plates, document a sharp cooling age discontinuity across the fault. This discontinuity could be interpreted as a difference in denudation history on each side of the fault. However, a low-relief Miocene erosional surface extends across the fault; this surface has been uplifted and incised and provides a geomorphic argument against differential denudation across the fault. By integrating magmatic, volcanic, and heat flow data, age-elevation profiles, and thermo-kinematic modeling, we propose that large horizontal displacement along the Motagua Fault has offset a persistent geothermal asymmetry across the fault and explains both the age discontinuities and the age-elevation patterns. This study illustrates how thermochronology can be used to detect large strike-slip displacements and more generally opens new perspectives in understanding the impact of nonuniform thermal structures on thermochronologic results.

1.   Introduction

[2]   Major strike-slip fault systems or wrench zones are commonly associated with large variations in denudation of orogenic crust [e.g., *Fitzgerald et al.*, 1995; *Storti et al.*, 2003; *Cruz et al.*, 2007; *Spotila et al.*, 2007; *Umhoefer et al.*, 2007; *Bermudez et al.*, 2011]. The contrasted cooling history of rocks that surround these faults as determined by thermochronometers is usually converted into contrasting exhumation rates assuming a uniform geothermal gradient [*Cruz et al.*, 2007; *Bermudez et al.*, 2011]. But large faults, such as transform plate boundaries, also juxtapose crustal blocks with contrasted thermal structures [*Le Pichon et al.*, 2005]. This juxtaposition creates strong lateral thermal gradients, which in turn favor strain localization and control the internal dynamics of strike-slip faults. Such variations in thermal structure across strike-slip faults had been largely described for oceanic transform faults [e.g., *Bouillin et al.*, 1997; *Sage et al.*, 2000; *Bigot-Cornier et al.*, 2005] and make the interpretation of denudation rates and deformation history problematic.

[3]   In this study, we evaluate quantitatively the impact on thermochronology patterns and age-elevation relationships using numerical modeling of (i) a pronounced geothermal asymmetry astride a major strike-slip fault and (ii) the associated lateral heat transfer through the strike-slip fault when the two different thermal setting are juxtaposed. Then, we confront modeling results with a natural example, the Motagua-Polochic Fault Zone (MPFZ), a 500 km long continental transform belonging to the boundary between the North American plate to the north and the Caribbean plate to the south (Figure 1A). We compile published thermochronological data (^{40}Ar-^{39}Ar and AFT data) [*Harlow et al.*, 2004; *Ratschbacher et al.*, 2009] and present

---

[1]Institut des Sciences de la Terre, Université Joseph Fourier – Grenoble 1, CNRS, Grenoble, France.

[2]Department of Earth and Environmental Sciences, University of Pennsylvania, Philadelphia, Pennsylvania, USA.

[3]Department of Earth Sciences, University of Minnesota, Minneapolis, Minnesota, USA.

[4]Geological Institute, Earth Science Department, Eidgenössische Technische Hochschule, Zürich, Switzerland.

[5]Department of Geosciences, University of Arizona, Tucson, Arizona, USA.

[6]Institut Universitaire Européen de la Mer, Université de Brest, Plouzané, France.

Corresponding author: T. Simon-Labric, Institut des Sciences de la Terre, Université Joseph Fourier – Grenoble 1, CNRS, BP53, FR-38041 Grenoble Cedex, France. (Thibaud.simon-labric@ujf-grenoble.fr)
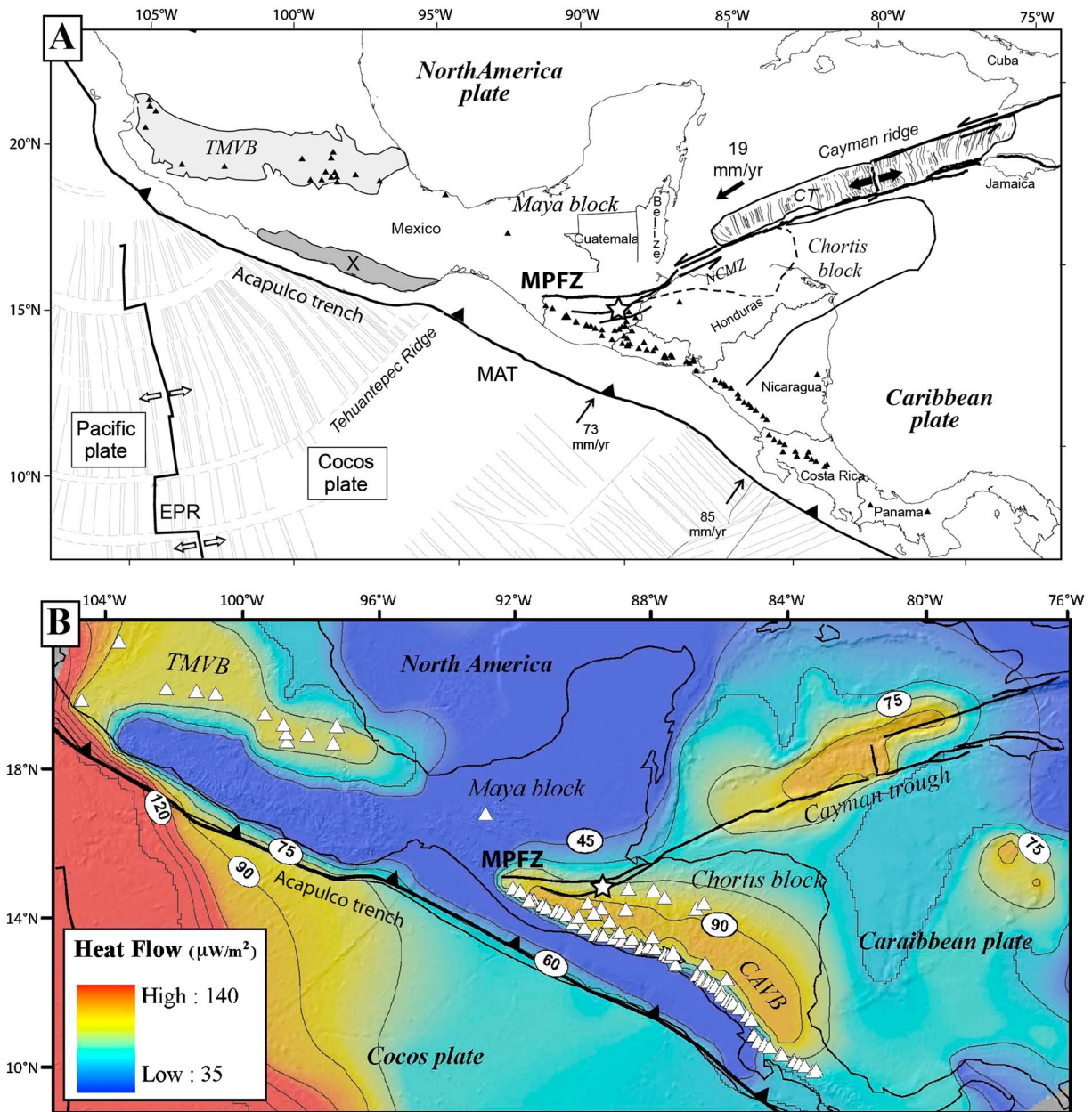
Figure 1. A) Tectonic setting of northern Central America and southern Mexico showing the location and names of main geologic features and tectonic contacts (modified from *Rogers and Mann* [2007]). CT—Cayman trough; EPR—East Pacific Rise; MAT—Middle America trench; MPFZ—Motagua-Polochic Fault Zone; NCMZ—Northern Chortís magmatic zone; TMVB—Trans-Mexican Volcanic Belt; X—Xolapa complex. B) Heat flow map of the North America-Caribbean plate boundary showing active volcanoes [modified from *Blackwell and Richards*, 2004]. White triangles are volcanoes, thick black lines are faults, thin black line is the coastline, and thin gray lines represent isovalues of surface heat flux. TMVB—Trans-Mexican Volcanic Belt; CAVB—Central American Volcanic Belt.

33 new zircon (U-Th)/He (ZHe) ages from 15 samples that were collected along age-elevation profiles on both sides of the fault trace. Finally, we compare the thermochronology data set with model predictions and discuss how geothermal asymmetry across the Motagua continental transform fault has influenced the cooling history and the thermochronologic record.

[4] Left-lateral displacements along the MPFZ initiated during the Late Cretaceous [e.g., *Pindell et al.*, 1988; *Pindell et al.*, 2005; *Pindell and Kennan*, 2009] and have accommodated a minimum displacement of ~1100 km since Middle Eocene time [*Rosencrantz et al.*, 1988]. The MPFZ separates the Chortís block to the south, a continental block that is now inserted into the otherwise dominantly oceanic Caribbean Plate, from the Maya block to the north, a continental block that belongs to the North American continent (Figure 1A). The present-day heat flow map [*Blackwell and Richards*, 2004] shows that the MPFZ is a
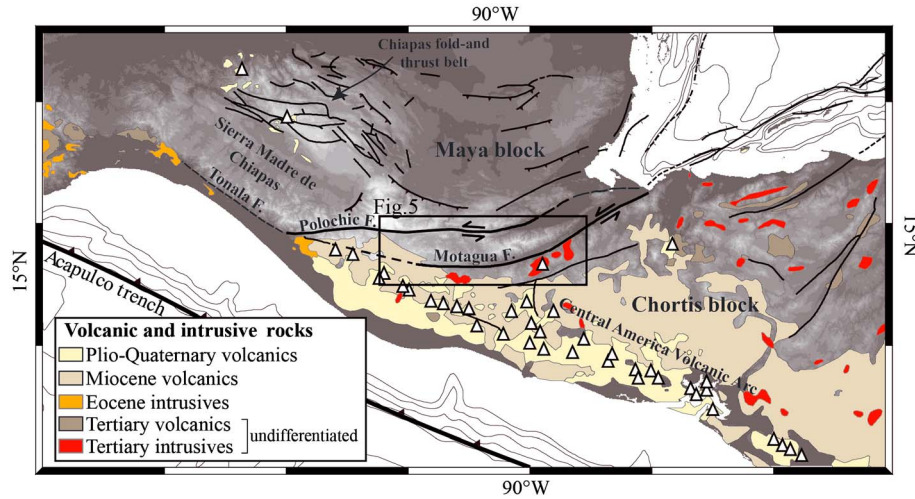
Figure 2. Simplified geologic map of northern Central America and southern Mexico showing the igneous activity since the Eocene, compiled from the 2005 Geologic Map of North America [*Reed et al.*, 2005]. Black lines are faults, white triangles are volcanoes. Middle-Late Miocene intrusions emplaced near the Tonala Fault [*Wawrzyniec*, 2005; *Witt et al.*, 2012] are too small to be shown.

major thermal boundary between the high heat flow Chortís block (surface heat flow ≥ 90 µW/m^2) to the south and the low heat flow Maya block (≤45 µW/m^2) to the north (Figure 1B). This translates into a short-distance transition in geothermal gradient from ~20°C/km north of the MPFZ to ~40°C/km south of the MPFZ, assuming a rock conductivity of 2.5 Wm^{-1} k^{-1} that is typical of continental crust [*Touloukian et al.*, 1981]. Cenozoic magmatism and present-day volcanic activity are also contrasted across the plate boundary (Figure 2). Modern volcanic activity is widespread at the western tip of the Chortís block, including the Central America Volcanic Arc [*Carr et al.*, 2003; *Bolge et al.*, 2009] and alkaline volcanism in the back arc [*Walker et al.*, 2011]. In contrast, volcanism is sparse along the southern edge of the Maya block and limited to few eruptive centers in the Sierra Madre de Chiapas [*García-Palomo et al.*, 2004; *Mora et al.*, 2007]. This asymmetric magmatic activity extends into the past, with episodic Miocene events north of the MPFZ, along the Polochic [*Ratschbacher et al.*, 2009] and Tonala faults [*Wawrzyniec*, 2005; *Witt et al.*, 2012], while nearly continuous, large-volume magmatism has characterized the Chortís block at least since Eocene time (Figure 2) [*Donnelly et al.*, 1990]. All these observations suggest that these two tectonics blocks sustained an asymmetric thermal evolution and that large-scale horizontal transfer along the MPFZ has juxtaposed a cooler northern block against a warmer southern block (Figure 1B). In the next section, we explore quantitatively the generic case of contrasting geotherms across a strike-slip fault.

2. Numerical Modeling

2.1. Model Description

[5] *Pecube* [*Braun et al.*, 2012] is a finite-element model that solves the transient advection-diffusion equation and is coupled with an age-prediction model that simulates landscape-evolution scenarios and predicts thermochronologic ages. For each sample locality and all surface nodes, particle

paths and corresponding time-temperature (*t-T*) histories are predicted. Thermochronological ages are calculated using the modeled *t-T* path, the annealing algorithm of *Stephenson et al.* [2006] for AFT ages, and diffusion models of *Reiners et al.* [2004] and *Hames and Bowring* [1994] for ZHe ages and white mica ^{40}Ar-^{39}Ar ages, respectively.

[6] Here we use a modified version of *Pecube*, which allows the thermal structure of the crust to vary spatially and temporally in order to explore the effect of geothermal variability on thermochronological ages. The thermal field within the model domain is controlled by radiogenic heat production, diffusion of heat from a fixed-temperature basal boundary, and advection of heat to the surface resulting from surface denudation as in the classic version of *Pecube*. The modified version includes an additional heat production parameter called *Ha*, which allows for changes in geothermal gradient while other parameters, such as denudation rate or topographic evolution, remain the same. The general heat-transport equation can be written as:

$$\rho c \frac{\partial T}{\partial t} + E \rho c \frac{\partial T}{\partial z} = k \nabla_2 T + H_r + H_a \qquad (1)$$

where *T* is temperature, *t* is time, *z* is the vertical spatial coordinate, *E* is the vertical rock uplift rate (i.e., the velocity of rocks with respect to the fixed base at z = -L), *k* is conductivity, *ρ* is crustal density, *c* is heat capacity, *Hr* is the rate of radiogenic heat production, and *Ha* is the rate of additional heat production. We only reproduce vertical displacement of rocks and do not simulate any deformation process, such as faulting.

[7] As illustrated by the surface heat flow map of the North America-Caribbean plate boundary (Figure 1B), the upper plate of a subduction system is characterized by a dynamic thermal structure that is controlled by mantle wedge processes, including magmatism [e.g., *Currie et al.*, 2004], in addition to tectonic and surface processes. *Ha* is used as a proxy for the addition of heat into the upper crust brought into the system by processes such as basal heating of the lithosphere, crustal

Table 1. Fixed Model Parameters

Parameters	Unit	Value
Crustal thickness	km	30
Nb of nodes in Z-direction		21
Crustal density	kg/m^3	2700
Mantle density	kg/m^3	3200
Poisson's ratio		0.25
Thermal diffusivity	km^2/Ma	25
Temperature at the model base	$°C$	450
Radioactive heat production	mW/m^3	1.1
Temperature at sea level	$°C$	20
Atmospheric lapse rate	$°C/km$	6
Young's modulus	N/m^2	10^{11}
Grid resolution	m	500

magma advection, and latent heat liberated during the conversion of melt to rock. Our approach has the strong advantage of being simple to implement, because geothermal variability is introduced without having to choose the origin of the heat. This point is important in a geologic setting like the Chortís block, where magmatic history is not known precisely. On the other hand, our model cannot simulate local perturbations to the thermal structure, or the deflection of isotherms produced by individual magmatic intrusions.

2.2. Numerical Simulation of a Geothermal Asymmetry and Lateral Heat Transfer Across a Major Strike-Slip Fault

[8] To illustrate the effect of the spatial variability of geotherm on thermochronology map patterns and age-elevation relationships across a major strike-slip fault, we conducted forward *Pecube* models that simulate the thermal evolution of two tectonic blocks with different geothermal gradients. In the warm block, an additional heat parameter Ha of $2.9\,\mu W/m^3$ is added uniformly and generates a geothermal gradient of 40°C/km. In the cool block, the additional heat parameter Ha is $0\,\mu W/m^3$, generating a geothermal gradient of 20°C/km. The basal model temperature, the radiogenic heat production, and the rate of vertical rock uplift are uniform and stable all along the model simulations ($Tb = 450°C$ at 30 km depth, $Hr = 1.1\,\mu W/m^3$, $E = 0.15$ km/Ma). Other constant parameters are listed in Table 1. Each modeled scenario is run for a flat topography and for a steady 2D sinusoid topography with a wavelength of 30 km and an amplitude of 2 km.

[9] Two tectonic scenarios are considered. In a first model, the two tectonic blocks with different geothermal gradients are simulated separately; cooling and a denudation precede their juxtaposition along the strike-slip fault (Figure 3). In the second model, the blocks are in contact at the initiation of the simulation, allowing for lateral heat transfer across the fault (Figure 4).

[10] The first model produces a sharp geothermal discontinuity astride the strike-slip fault (Figure 3A). Heating of the warm block imposes a rise of isotherms toward the topographic surface; the closure temperature isotherms are twice as close to the surface as in the colder block, and cooling ages are about twice as young (AFT = ~12–20 Ma instead of 27–39 Ma; ZHe = ~24–33 Ma instead of 48–63 Ma, muscovite ^{40}Ar-^{39}Ar = ~49 Ma instead of 82). In first order, age-elevation relationships are translated toward younger ages in the hot block (Figure 3C). Under the warm block, the deflection of isotherms under the

topographic surface is more pronounced and translates into a stronger exaggeration of the apparent exhumation rates. This effect has been fully described for low-temperature thermochronology (AHe, AFT) [*Braun*, 2002; *Braun et al.*, 2006]. We show here that it can affect higher temperature thermochronometers as well, such as ZHe if the geothermal gradient is sufficiently high, like in the Chortís block (~40°C/km). The numerical simulation demonstrates that variability of geothermal gradient on its own can control variability of thermochronological ages and for its amplitude. Ignoring the role of the thermal setting of such tectonic area would lead to erroneous interpretation of the age patterns, for example interpreting them in terms of differences in denudation rates.

[11] The second model adds the effect of lateral heat transfer across the strike-slip fault, simulating a tectonic setting in which the horizontal displacement along the strike-slip fault had been sufficient to place in contact these two blocks with a different thermal structure (Figure 4A). A ~30 km wide, horizontal thermal transition is generated, centered on the fault. At the fault itself, the thermochronological ages equal the mean value of each system in adjacent blocks (Figure 4B). The lateral transfer of heat modifies the age-elevation relationships, producing slope steepening in the hot block and slope shallowing in the cool block (Figure 4C). Note that the sampling strategy of the "vertical" profile is currently used to estimate denudation rates assuming that the thermal structure does not vary laterally along the profile [*Fitzgerald et al.*, 1995]; this assumption is not respected in this case. The occurrence of old thermochronological ages and slow apparent denudation rates derived from age-elevation relationships on one side of the fault, and younger ages with higher apparent denudation rates on the other side of the fault, records thermal exchange through the strike-slip fault that separates two thermal blocks; these relationships could be erroneously interpreted as recording a differential denudation history. In the following sections, we use these numerical model results to guide our interpretation of the thermochronological data around the MPFZ.

3. The MPFZ

3.1. Tectonics of the Plate Boundary Since Eocene Time

[12] The 3500 km long northern Caribbean plate boundary accommodates westward motion of North America relative to the Caribbean Plate (Figure 1A) [*DeMets et al.*, 2000]. Over its length, the plate boundary is mostly left lateral, except in the Cayman Trough, where a short spreading center, perpendicular to the overall strike of the plate boundary, lies in the middle of a 1200 km long pull-apart basin. Oceanic accretion in the basin is thought to have started at 30 Ma [*MacDonald and Holcombe*, 1978], or 49 – 50 Ma [*Rosencrantz et al.*, 1988; *Leroy et al.*, 2000]. The spreading center efficiently transfers most of the ~2 cm/yr left-lateral plate motion [*DeMets et al.*, 2000].

[13] Further to the west in Guatemala, the transform boundary is a zone of diffuse deformation that consists of several major transcurrent faults; from south to north, these are the Jocotán-Chamelecón Fault, the Motagua Fault, and the Polochic Fault (Figure 5) [e.g., *Donnelly et al.*, 1990; *Guzmán-Speziale*, 2010; *Authemayou et al.*, 2011]. The

A)

Cool block

Hot block

Isotherms

100
200
300
400

$G \approx 20°C/km$

$G \approx 40°C/km$

$E=150\ m/Ma$

$E=150\ m/Ma$

10   200   400   600

Temperature (°C)

B)

Cool block

Hot block

Strike-slip fault

Thermochronological ages (Ma)

80 — Musc. Ar-Ar

70

60

50 — ZHe

Musc. Ar-Ar

40

ZHe

30 — AFT

AFT

20

10

0   20   40   60   80   100   120   140

Horizontal distance (km)

C)

Elevation (m)

3000

ZHe
316 m/Ma

AFT
418 m/Ma

AFT
241 m/Ma

2000

ZHe
198 m/Ma

1000

0

0   10   20   30   40   50   60   70
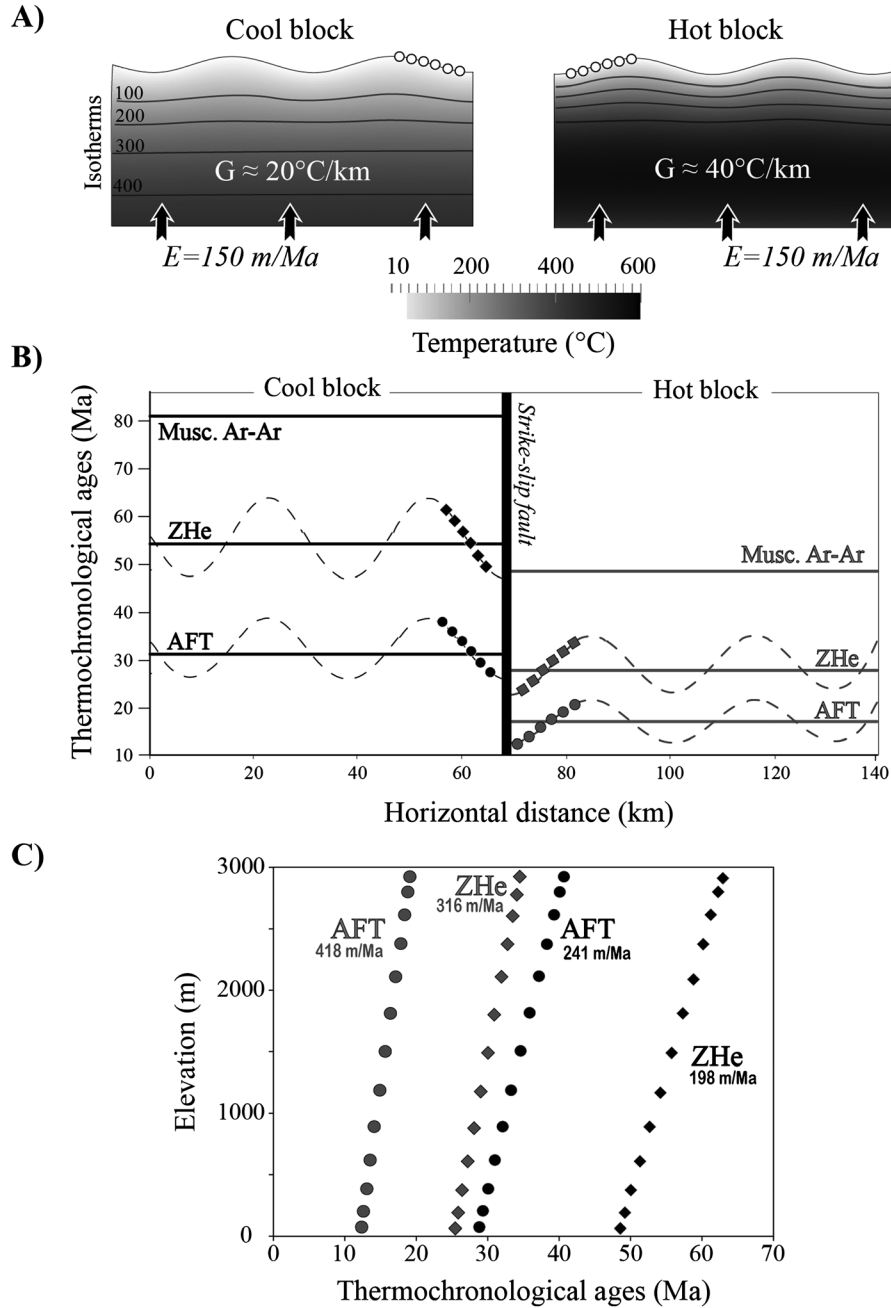
Thermochronological ages (Ma)

Figure 3. Thermal structure of two tectonic blocks with different geothermal gradients separated by a large strike-slip fault, and cross sections with synthetic ZHe/AFT ages. The two tectonic blocks are simulated separately in order to reproduce the thermal evolution of the two tectonic blocks, which have cooled before to being juxtaposed by the horizontal displacement along the strike-slip fault. (A) Model thermal structure (isotherms in °C) for a steady-state sinusoidal topography with wavelength $\lambda = 30$ km, amplitude $A = 2$ km, and a constant 150 m.Ma^{-1} denudation rate. See Table 1 for other thermo-kinematic parameters used in *Pecube* modeling. (B) Predicted ZHe (diamonds) and AFT (dots) age-horizontal distance profiles collected across the strike-slip fault. Solid lines show results for a flat topography and dashed line results for steady-state sinusoidal topography. (C) Predicted ZHe (diamonds) and AFT (dots) age-elevation profiles collected in both tectonic blocks. Black symbols come from the cool block (~20°C/km) and white symbols from the hot block (~40°C/km). Note that synthetic ^{40}Ar-^{39}Ar ages are not represented because real ^{40}Ar-^{39}Ar ages do not give clear age-elevation trends.

Motagua Fault is the direct topographic and structural continuation of the southern Cayman trough (Figure 1). GPS measurements fitted to a model of elastic deformation suggest that the Motagua Fault accommodates ~75% of the interplate motion [*Lyon-Caen et al.*, 2006]. The fault ruptured over 230 km in dominantly strike-slip motion in 1976 [*Plafker*, 1976]. Unlike the other two strike-slip faults of the boundary, the Motagua Fault trace is smooth

A)

Cool block

Motagua valley width=30km

Hot block

100
200
300
400

G ≈ 20°C/km

Motagua fault

G ≈ 40°C/km

0   20   40   60   80   100   120   140

E=150 m/Ma

10   200   400   600

Temperature (°C)

B)

Cool block

Hot block

Musc. Ar-Ar

Lateral heat transfer area

Strike-slip fault

ZHe

AFT

Thermochronological ages (Ma)

80
70
60
50
40
30
20
10

0   20   40   60   80   100   120   140

Horizontal distance (km)

C)

AFT   ZHe   ZHe
194 m/Ma   446 m/Ma   193 m/Ma

AFT
506 m/Ma

Elevation (m)

3000
2000
1000
0

0   10   20   30   40   50   60   70
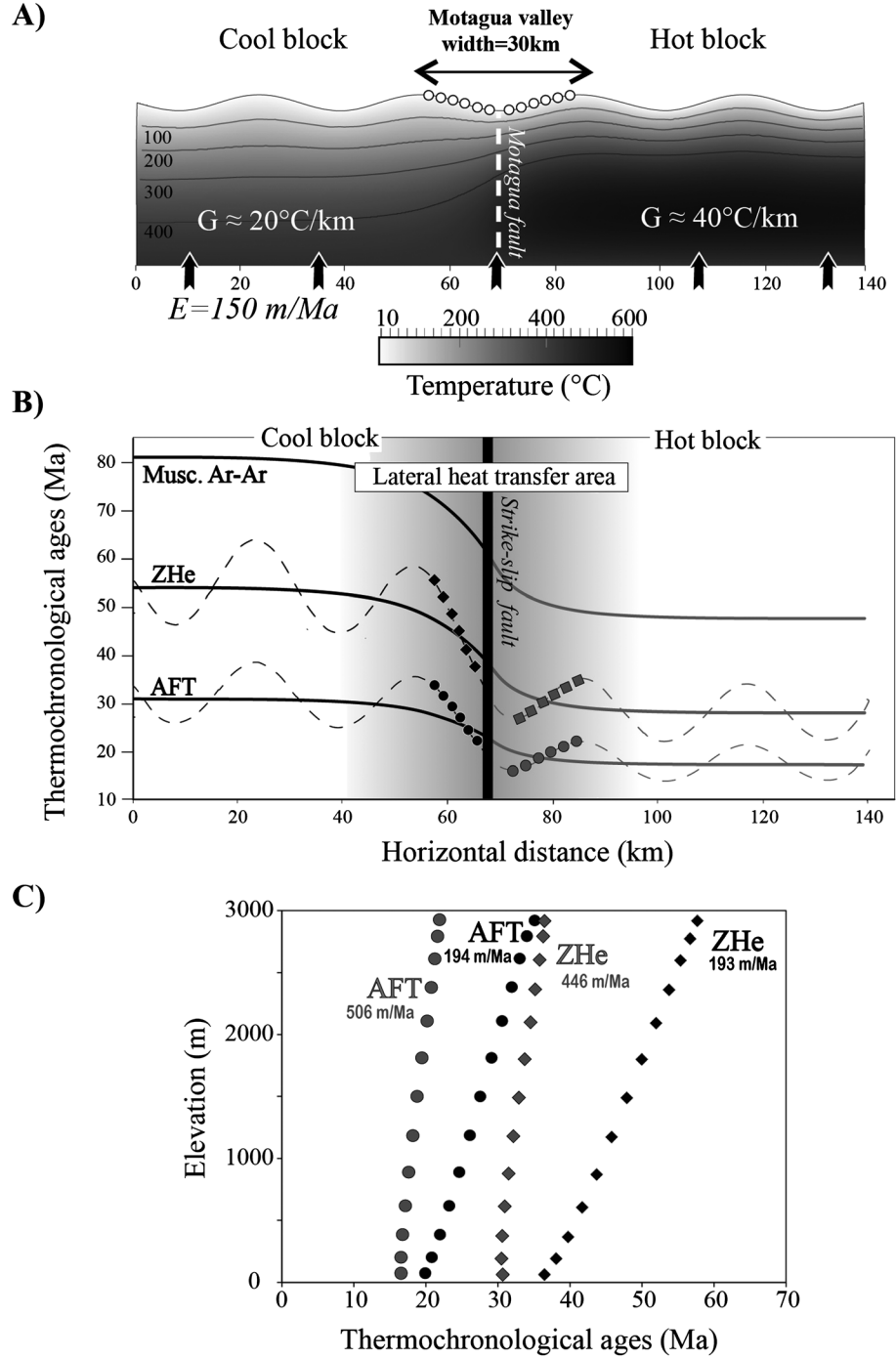
Thermochronological ages (Ma)

Figure 4. Thermal structure of two tectonic blocks with different geothermal gradients separated by a large strike-slip fault, and cross sections with synthetic ZHe/AFT ages. The two blocks are in contact since initiation of the simulation at 85 Ma, introducing a horizontal thermal gradient and therefore thermal equilibrium astride the two blocks. (A) Model thermal structure (isotherms in °C) for steady-state sinusoidal topography with wavelength $\lambda = 30$ km, amplitude $A = 2$ km, and a constant 150 m Ma^{-1} denudation rate. See Table 1 for other thermo-kinematic parameters used in *Pecube* modeling. (B) Predicted ZHe (diamonds) and AFT (dots) age-horizontal distance profiles collected astride the strike-slip fault. Solid lines show results for a flat topography, and dashed lines show results for the steady-state sinusoidal topography. (C) Predicted ZHe (diamonds) and AFT (dots) age-elevation profiles collected in both tectonic blocks. Black symbols come from the cool block (~20°C/km) and white symbols from the hot block (~40°C/km).
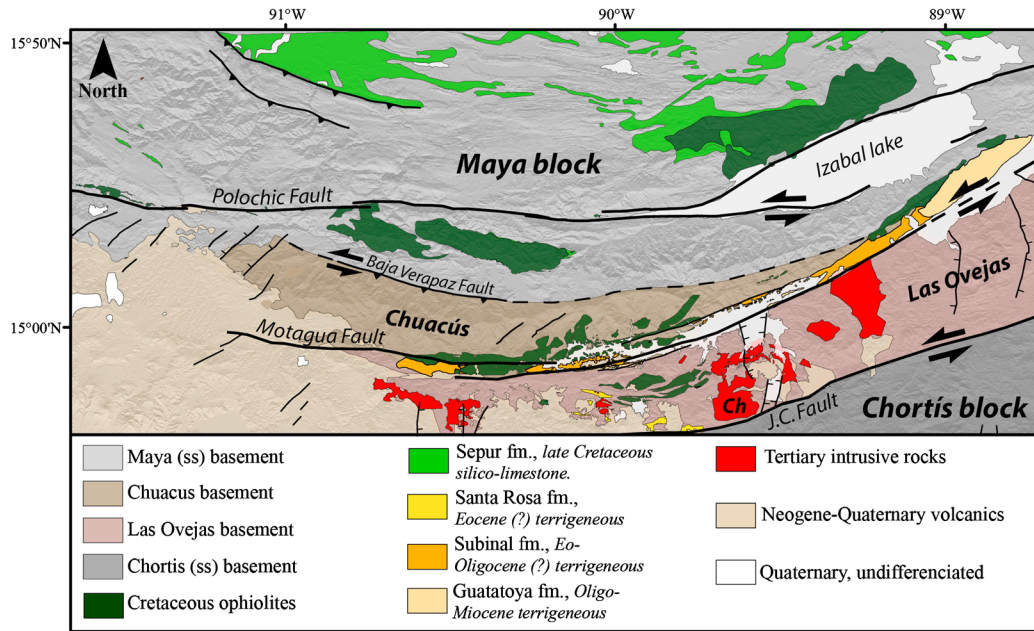
Figure 5. Simplified geologic map of the Motagua-Polochic Fault Zone (compiled after *Anderson et al.* [1985], *Buckart et al.* [1987], *Donnelly et al.* [1974], *Kesler et al.* [1970], *McBirney* [1963], *Brocard et al.* [2011], and *Authemayou et al.* 2011)). Ch—Chiquimula batholith; J.C. Fault—Jocotan-Chameleon Fault.

[Schwartz *et al.*, 1979] and tracks serpentinized ophiolitic bodies [*Donnelly et al.*, 1990].

[14] The Polochic Fault, 50 km further north, likely branches onto the Motagua Fault in the Caribbean Sea to the east (Figure 1). The Polochic Fault has an abundant record of large historical earthquakes [*White*, 1984; *White*, 1985], but GPS measurements [*Lyon-Caen et al.*, 2006] indicate that the fault currently takes up no more than 25% of interplate motion. The Jocotán-Chamelecón Fault, located 30–40 km south of the Motagua Fault is inactive, and unlike the other two faults, does not directly connect with the Cayman Trough [*Schwartz et al.*, 1979].

[15] It has been suggested that plate motion has switched from one fault to the other [*Burkart*, 1983; *Deaton and Burkart*, 1984; *Burkart*, 1994; *Rogers and Mann*, 2007], but the Motagua Fault has remained the major boundary for most of the time since the Eocene. Field evidence indicates that the Jocotán-Chamelecón Fault has not experienced any major strike-slip activity since at least 20 Ma [e.g., *Clemons*, 1966; *Donnelly et al.*, 1990; *Muehlberger and Ritchie*, 1975], and possibly since Cretaceous time [*Ritchie*, 1976]. Facies changes in carbonate sequences near the fault suggest Albian fault activity [*Donnelly et al.*, 1990]. The presence of Cretaceous carbonate (Valle de los Angeles formation) on both sides of the Jocotán-Chamelecón Fault also suggests limited motion of this very fragmented fault since that time [*Authemayou et al.*, 2012]. Before the large 1976 earthquake on the Motagua Fault, the Polochic Fault was regarded by some as the major plate boundary [*Kesler*, 1970; *Donnelly et al.*, 1974; *Muehlberger and Ritchie*, 1975]. The total offset of the Polochic Fault was initially evaluated to be <150 km [*Kesler*, 1970], then more precisely 132 ± 5 km, based on the offset of Paleocene-Eocene folds [*Burkart*, 1978]. The total offset on the fault is far less than the 750–1500 km opening distance of the Cayman Trough [*Holcombe et al.*, 1990; *LeRoy et al.*,

2000]. These observations altogether suggest that the Motagua Fault is the weakest fault in the system and is indeed the most likely to accommodate much of the transcurrent motion.

3.2. Terrane Evolutions Across the Plate Boundary

[16] High-pressure/low-temperature ophiolitic rock belts crop out within 20 km on both sides of the Motagua Fault and define the Motagua suture zone [e.g., *Beccaluva et al.*, 1995; *Harlow et al.*, 2004; *Martens et al.*, 2012; *Ortega-Gutiérrez et al.*, 2007; *Ortega-Obregon et al.*, 2008; *Ratschbacher et al.*, 2009]. About half of these belts consist of serpentinite bodies [e.g., *McBirney*, 1963; *Donnelly et al.*, 1990; *Beccaluva et al.*, 1995]. These Early Cretaceous rocks [*Brueckner et al.*, 2009] were exhumed to upper crustal levels at ~110–120 Ma south of the fault (modern coordinates), and between ~75 and 55 Ma north of the fault [*Harlow et al.*, 2004; *Brueckner et al.*, 2009]. The ophiolites are thrust onto two elongate terranes.

[17] The terrane that borders the Motagua Fault to the north is the Chuacús complex, a continental terrane, which today belongs to the Maya block and is made of a core of micaschist and gneiss, fringed by more diverse assemblages of amphibolite, marble, and migmatite [*McBirney*, 1963]. Garnet-clinopyroxene-phengite thermobarometry of Chuacús gneisses indicates eclogitic conditions to ~700°C and ~2.1–2.4 GPa. U-Pb dating of eclogite metamorphic zircon yielded a 75.5 ± 2 Ma age [*Martens et al.*, 2012]. The Chuacús complex then was retrogressed to amphibolite grade [*Ratschbacher et al.*, 2009]. The ages of the eclogite-facies event and the amphibolite-facies retrogression are equivalent [*Martens et al.*, 2012]. Thus, exhumation of the Chuacús complex from mantle to midcrustal depth was quick, taking few million years. During exhumation, Chuacús gneisses was intruded by ~76–66 Ma pegmatite according to U-Pb, Rb-Sr, and K-Ar ages [*Ratschbacher*
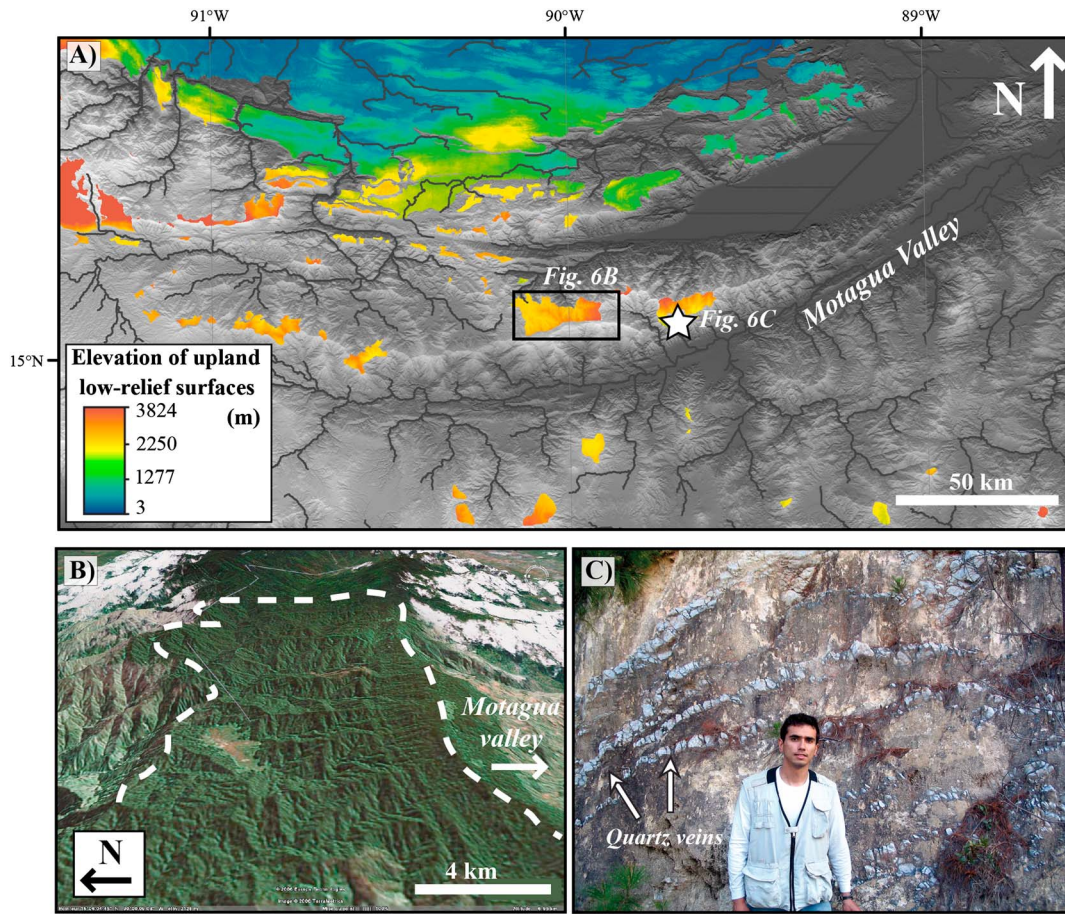
Figure 6. A) Shaded relief map (SRTM 90 m) showing remnants of low-relief high-elevation surfaces. The surface remnants have been mapped manually and are color coded according to their elevation. Black box shows the location of the area view in Figure 6B. White star shows location of the saprolite in Figure 6C. B) Relict landscape on Chuacus basement, areal view looking to the East. White dashed line is paleo-relief border. C) Strong chemical alteration of saprolite showing quartz veins.

et al., 2009; *Martens et al.*, 2012] and deformed by ductile left-lateral wrenching [*Kesler*, 1970; *Donnelly et al.*, 1990]. The complex cooled from 550°C (hornblende ^{40}Ar-^{39}Ar) to 275°C (biotite ^{40}Ar-^{39}Ar) between ~75 and 65 Ma [*Sutter*, 1979; *Ortega-Gutiérrez et al.*, 2004; *Ratschbacher et al.*, 2009]. The Chuacús complex belongs to the North American continent but is separated from the rest of the Maya block further north by a ductile shear zone, the Baja Verapaz Fault (Figure 5), that accommodated an unknown amount of reverse-lateral displacement [*Ortega-Obregon et al.*, 2008]. North of the Baja Verapaz Fault, the basement of the Maya block consists of weakly metamorphic Early Paleozoic sedimentary rocks intruded by Ordovician plutons and covered by nonmetamorphic Mississipian to Cretaceous continental to marine sedimentary units [*Weber et al.*, 2007; *Ortega-Obregon et al.*, 2008; *Witt et al.*, 2012].

[18] To the south, the Las Ovejas complex borders the northern limit of the Chortís block. The Las Ovejas rocks can be subdivided into metamorphosed volcanosedimentary rocks and granitic components. The former includes interlayered quartzofeldspathic gneisses, schists, marbles, and amphibolites containing mineral assemblages indicative of midamphibolite facies conditions [*Ratschbacher et al.*,

2009]. The metagranitic component includes metamorphosed intrusives of dioritic to granodioritic composition, granitic dikes, and deformed pegmatites. Amphibolite-facies conditions, migmatization, intrusions, and deformation occurred between ~27 and ~37 Ma [*Torres de León et al.*, 2012]. This event masked earlier Permo-Triassic and Jurassic high-grade events and their associated intrusions and migmatization [*Ratschbacher et al.*, 2009]. To the south of the Las Ovejas complex, the terrane is separated from the rest of the Chortís block by the Jocotán-Chamelecón Fault (Figure 5).

[19] In summary, the two sides of the Motagua Fault exhibit contrasted metamorphic and deformation histories: to the north, the elongate Chuacús terrane was strongly deformed [*Kesler*, 1970; *Donnelly et al.*, 1990], rapidly exhumed to upper crustal levels and invaded by upper-crustal pegmatites in Late Cretaceous [*Ratschbacher et al.*, 2009; *Martens et al.*, 2012]. In contrast, the Las Ovejas complex to the south has experienced Eocene-Oligocene metamorphism and deformation as a result of its displacement off southern Mexico that was mainly accommodated by sinistral shearing and Cenozoic tectonic transport [*Torres de León et al.*, 2012].
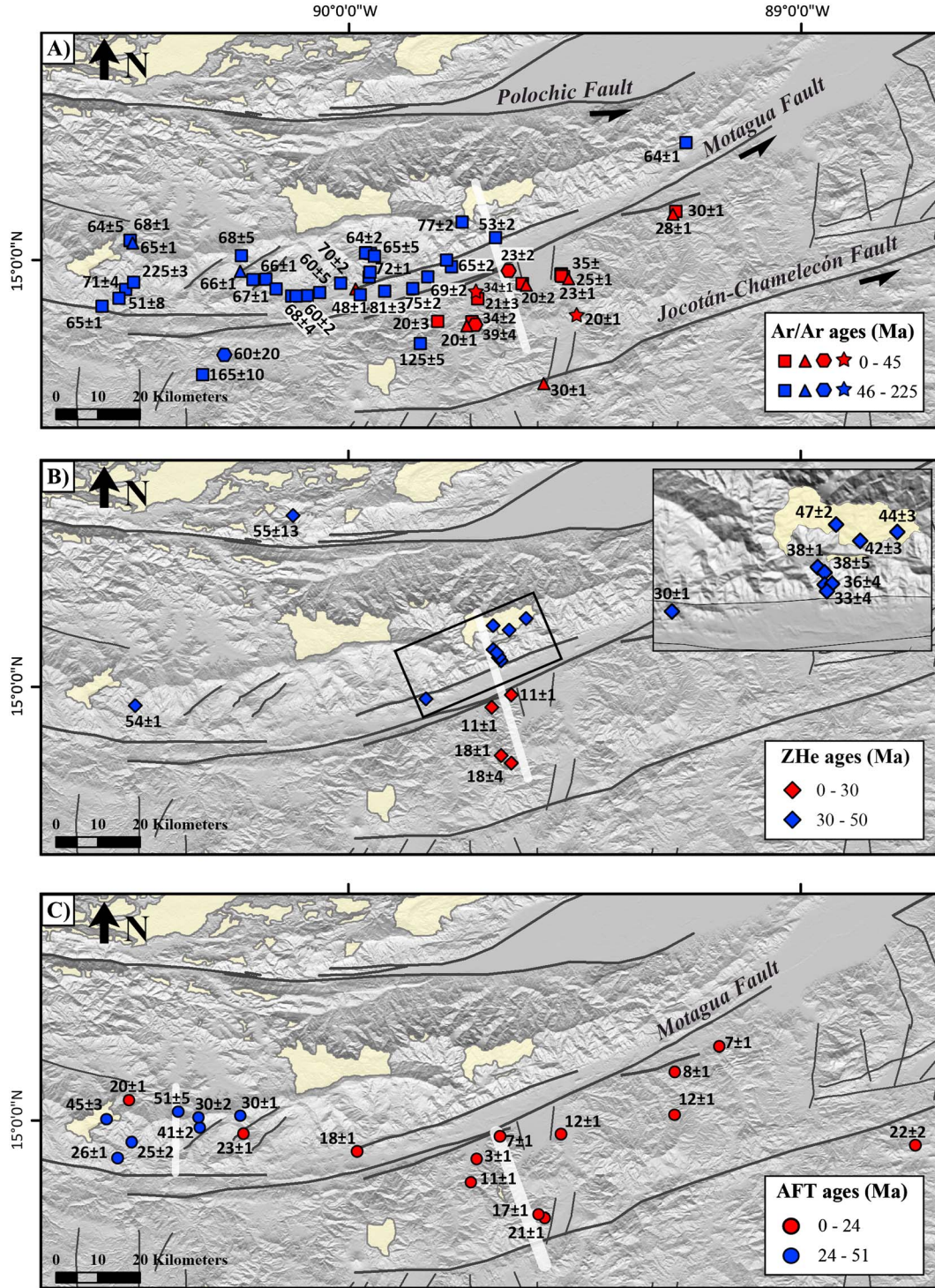
Figure 7. Shaded relief map (SRTM 90 m data) showing sample locations and thermochronologic ages. Light gray lines indicate topographic cross sections on Figure 8. Maps are arranged from lower to higher temperature sensitive thermochronometers: A) Published ^{40}Ar-^{39}Ar and K-Ar ages [*Ortega-Gutiérrez et al.*, 2004; *Harlow et al.*, 2004; *Ratschbacher et al.*, 2009]; squares are muscovite ages (closure temperature of ~350°C); triangles are biotite ages (~300°C), hexagon are hornblende ages (~500°C), and stars are feldspath ages (~250°C); B) new zircon (U-Th)/He ages (~190°C); C) published apatite fission track (AFT) ages (~110°C) [*Ratschbacher et al.*, 2009]. Low-relief high-elevation surfaces (Cf. Figure 6) are shown in yellow.
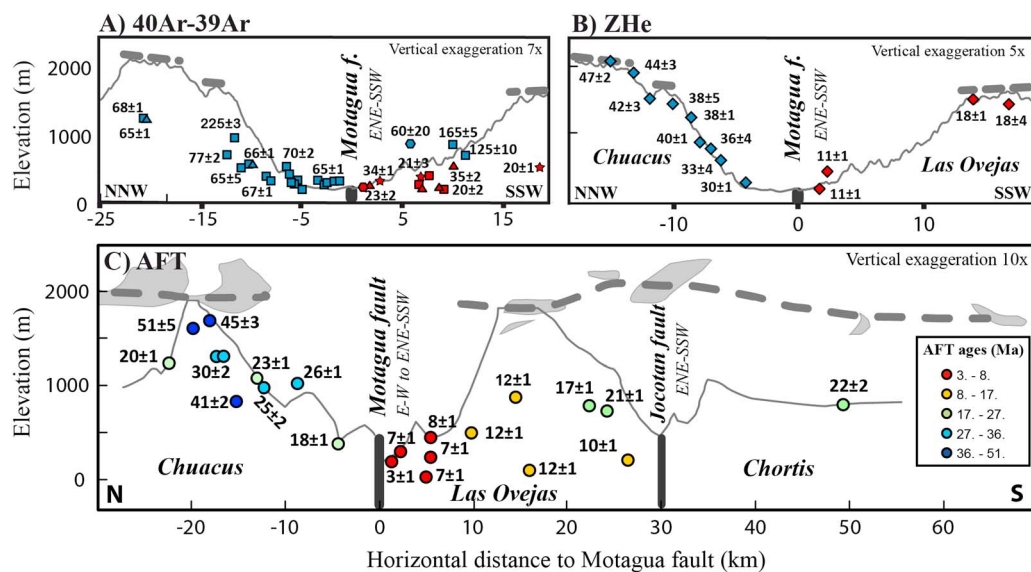
Figure 8. Geological cross sections with thermochronologic ages of Maya and Chortís blocks; A) $^{40}Ar/^{39}Ar$, B) ZHe, and C) AFT ages are projected along horizontal distance from the Motagua Fault. Age color coding and topographic profiles located in Figure 7. Gray surfaces are projections of landscape relicts along the topographic profile, and shade gray line is the paleo-relief reconstruction.

3.3. Magmatic, Volcanic, and Thermal Settings on Either Side of the Motagua Fault

[20] The two sides of the Motagua Fault exhibit contrasted igneous and thermal histories. South of the Motagua Fault, the Chortís block has been affected by voluminous volcanic activity since at least Eocene time [*Donnelly et al.*, 1990]. Modern calc-alkaline volcanism is very active and forms the Central American Volcanic Arc [*Carr and Stoiber*, 1990], along the western edge of the Chortís block (Figure 2). Volcanic activity is recorded up to 150 km behind the main volcanic arc. This back-arc basaltic alkaline volcanism is widespread and has formed extensive monogenetic cone fields and some stratovolcanoes between the volcanic arc and the MPFZ [e.g., *Walker et al.*, 2011]. In the past, igneous activity of the Chortís block was also very active and punctuated by large Eo-Oligocene and Miocene ignimbritic flare-ups in the volcanic arc [*Jordan et al.*, 2007]. Across the northern part of the Chortís block, Late Cretaceous to early Cenozoic magmatism defines a broad swath (100 km wide) of magmatism [*Horne et al.*, 1976; *Kozuch*, 1991]. Aeromagnetic data in Honduras show a magnetic anomaly that has been interpreted as the associated intrusive belt referred to here as the Northern Chortís magmatic zone [*Rogers et al.*, 2007]. This belt crosses the west termination of the Las Ovejas complex, which has been nearly continuously intruded by large volumes of magma between 40 and 20 Ma (Figure 5) [*Ratschbacher et al.*, 2009]. Further east, the southern wall of the Cayman Trough exposes plutonic and volcanic rocks of Paleocene and Eocene age [*Holcombe et al.*, 1990] that are regarded as the oriental limit of the continental Chortís terrane.

[21] North of the Motagua Fault, some igneous activity is also evident but is characterized by episodic and low-volume activity (Figure 2): (1) middle-late Miocene intrusions within the Permian basement [*Wawrzyniec*, 2005; *Witt et al.*, 2012]; (2) subduction related Plio-Quaternary volcanism in a zone bounding the Central Depression and the High Sierra; and (3) recent volcanism related to the El Chichon volcano along

the North Deformational Front [*García-Palomo et al.*, 2004; *Mora et al.*, 2007]. From the middle-late Miocene, arc volcanism that started in the Sierra de Chiapas showed restricted activity and coeval inland migration from the Tonala Fault toward the Chiapas fold-and-thrust belt (Figure 2).

[22] The present-day heat flow map [*Blackwell and Richards*, 2004] shows a similar thermal asymmetry astride the MPFZ, which tectonically juxtaposes the high heat flow Chortís block to the south against the low heat flow Maya block to the north (Figure 1B). Locally, in the Chortís block, heat flow values exceed $250 \mu W/m^2$ [*Meert and Smith*, 1991], suggesting that active arc magmatism in the Chortís block participates to this thermal anomaly.

3.4. Geomorphology and Recent Deformation

[23] The disparity of deformation, igneous, and thermal histories recorded on either side of the Motagua Fault contrasts with the similarity of large-scale geomorphologic markers across the fault. The Motagua Fault is the location of a long valley that tracks the fault over its entire length and is presently occupied by the Motagua River (Figure 6). On either side of the Motagua valley, landscape exhibits extensive, low-relief relict erosional surfaces, now found on top of the most elevated mountains. North of the Motagua Fault, the upland surface is well defined and stands some 2000 m above the river floor [*Authemayou et al.*, 2011; *Brocard et al.*, 2011]. The upland surface is mantled by a thick (~100 m) saprolite developed over the crystalline rocks of the Chuacús complex (Figure 6C). The surface started being perched and dissected in the Late Miocene, between 12 and 7 Ma [*Brocard et al.*, 2011]. On the Chortís block, an extensive paleosurface of both erosional and depositional origin, thought to have formed as a low, rolling country, not far above sea level [*Williams and McBirney*, 1969], is now buried below >2 km thick ignimbrite sheets that were deposited during a Miocene volcanic flare-up that peaked between 17 and 13 Ma [*Sigurdsson et al.*, 2000; *Jordan et al.*, 2007]. Subsequent uplift and incision of the

Table 2. Zircon (U-Th)/He Ages From the Motagua-Polochic Fault Zone[a]

Profile	Sample	Easting	Northing	Elev.	[4]He	U	Th	Raw age	F_T	Corr. Age	Error	Lab
		(decimal degrees)	(decimal degrees)	(m)	ncc/g	(ppm)	(ppm)	(Ma)		(Ma)	(Ma)	
San Lorenzo	10-51z2	15.11947	−89.68592	2220	5501125.19	1443.57	218.55	30.4	0.66	45.7	1.7	ETH-Z-Z
San Lorenzo	10-51z4	"	"	"	4485585.64	1065.08	184.54	33.4	0.68	49.1	1.2	UofA
										47.4	**2.3**	
San Lorenzo	11-11z1	15.06777	−89.68684	1468	425548.32	130.23	60.81	24.3	0.69	35.1	1.2	ETH-Z-Z
San Lorenzo	11-11z3	"	"	"	482095.38	105.83	65.63	32.8	0.79	41.6	0.9	ETH-Z
		"	"							**38.3**	**4.6**	
San Lorenzo	11-71z1	15.05106	−89.67471	923	1393074.17	402.81	153.27	26.2	0.68	38.7	0.9	ETH-Z
San Lorenzo	11-71z3	"	"	"	1347577.71	404.42	84.24	26.2	0.77	34.1	0.8	ETH-Z
										36.4	**3.2**	
San Lorenzo	11-81z1	15.04392	−89.66888	635	1981306.92	584.80	225.32	25.7	0.78	33.1	0.9	ETH-Z
San Lorenzo	11-81z2	"	"	"	1157806.9	321.53	196.44	26.0	0.72	36.0	0.8	ETH-Z
San Lorenzo	11-81z4	"	"	"	839907.06	290.10	166.65	21.1	0.71	29.7	0.6	ETH-Z
										32.9	**4.4**	
San Lorenzo	46-5z2	15.05132	−89.67309	833	6476028.54	1781.91	565.33	27.9	0.71	39.6	1.9	ETH-Z
San Lorenzo	46-5z3	"	"	"	1258464.49	278.40	95.98	35.3	0.86	41.3	0.6	UofA
										40.4	**1.2**	
San Lorenzo	46-8z1	15.06125	−89.67835	1247	2180891.79	551.85	180.54	30.3	0.77	39.2	1.2	ETH-Z
San Lorenzo	46-8z2	"	"	"	1122631.47	317.89	113.92	26.9	0.72	37.2	1.1	ETH-Z
										38.2	**1.4**	
San Lorenzo	47-72z1	15.13407	−89.61218	1934	3062210.48	706.64	204.02	33.5	0.74	45.3	0.4	ETH-Z
San Lorenzo	47-72z2	"	"	"	3287812.57	729.55	217.15	34.8	0.8	43.7	0.9	ETH-Z
										44.5	**1.2**	
San Lorenzo	47-142z1	15.1094	−89.6003	1575	4980054.48	1208.39	262.1	32.4	0.73	44.3	1.1	ETH-Z
San Lorenzo	47-142z2	"	"	"	3053247.53	818.12	154.04	29.5	0.74	39.7	1.3	ETH-Z
										42.0	**3.3**	
San Lorenzo	47-145z1	14.96282	−89.83603	355	905337.97	353.33	88.73	20	0.65	31.0	1.6	ETH-Z
San Lorenzo	47-145z2	"	"	"	905472.71	368.06	115.12	18.9	0.64	29.5	1.7	ETH-Z
										30.2	**1.1**	
Chiquimula	16-11z1	14.84084	−89.67217	1584	578372.99	396.74	215.32	10.7	0.77	13.9	1.0	ETH-Z
Chiquimula	16-11z4	"	"	"	756509.41	404.00	410.20	12.7	0.73	17.7	0.3	UofA
Chiquimula	16-11z5	"	"	"	627950.12	360.49	268.30	12.5	0.71	17.8	0.3	UofA
Chiquimula	16-11z2	"	"	"	830287.61	308.98	397.79	17.3	0.74	23.7	0.3	UofA
										18.3	**4.0**	
Chiquimula	16-21z4	14.82384	−89.64942	1396	8788.37	2.94	9.53	14.0	0.75	18.5	1.3	ETH-Z
Chiquimula	16-21z3	"	"	"	279006.85	158.40	136.07	12.3	0.75	16.7	0.3	UofA
										17.6	**1.3**	
Chiquimula	16-91z1	14.96998	−89.69784	249	435735.56	428.43	89.39	8.0	0.7	11.5	0.3	ETH-Z
Chiquimula	16-91z2	"	"	"	249079.82	275.74	48.74	7.3	0.72	10.2	0.2	UofA
										10.9	**0.9**	
Chiquimula	16-111z1	14.94399	−89.69137	510	511369.86	564.17	36.14	7.4	0.67	11.1	0.3	ETH-Z
Chiquimula	16-111z2	"	"	"	551157.94	571.71	125.49	7.6	0.64	11.9	0.3	ETH-Z
										11.5	**0.6**	
Polochic	9-111z3	15.351	−90.125	1023	2198346.83	352.41	100.31	48.2	0.75	64.0	1.9	UofA
Polochic	9-111z1	"	"	"	803062.67	191.23	46.28	32.8	0.71	46.2	1.1	UofA
										55.1	**12.6**	
El Chol	43-01z1	14.965	−90.4866	1041	598592.44	105.72	24.29	44.3	0.81	55.0	1.3	UofA
El Chol	43-01z3	"	"	"	715441.35	122.66	49.37	43.9	0.82	53.9	1.2	UofA
										54.5	**0.8**	

[a]Analytical uncertainty on U and Th determinations is ~3%. Abbreviations: Raw He age: grain age before applying the FT alpha-ejection correction factor; FT: correction factor for alpha ejection [*Hourigan et al.*, 2005] assuming homogeneous U and Th distribution; Corr He age: grain age after applying the FT alpha-ejection correction factor. The weighted-mean age for each sample is given in bold together with the error calculated from the 1σ standard deviation of the sample. San Lorenzo is the profile from the eastern Chuacus and Chiquimula from the eastern Las Ovejas, both profiles located in the Motagua Valley. El Chol sample comes from the western Chuacus and Polochic from the north side of the Polochic Fault.

Chortís block have been interpreted as the buoyant response of the upper plate to an influx of mantle asthenosphere following break-off and sinking of the Cocos plate slab after ~10 Ma [*Rogers et al.*, 2002]. In association with, or following this long-wavelength uplift, numerous north-south trending graben have grown in the Chortís block and disrupted its topography since late Miocene time (by ~10.5 Ma) [*Dengo et al.*, 1970; *Rogers et al.*, 2002; *Jordan et al.*, 2007]. Horst-and-graben displacements make mapping of the relict surfaces more difficult than on the Maya block. We restricted our mapping to a few surface remnants (Figure 6), where the erosional surface is easily distinguishable from the widespread depositional surfaces of Miocene ignimbrite sheets and more recent detrital accumulations. These relict features are useful for thermochronologic analysis because they constrain the Neogene topographic evolution and the amplitude of the regional incision along the Motagua valley since ~10 Ma.

3. Thermochronological Dating

3.1. Compilation of Existing Thermochronological Ages

[24] The [40]Ar-[39]Ar ages on K-feldspath, biotite, muscovite, and hornblende show a clear-cut separation between the two
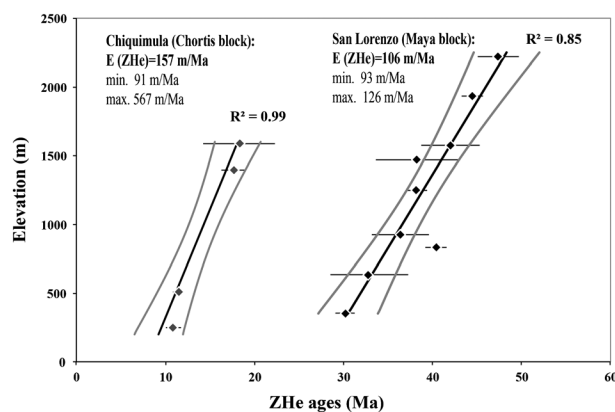
Figure 9. Age-elevation plots of San Lorenzo (Chuacús block) and Chiquimula (Las Ovejas block) profiles for zircon (U-Th)/He data with weighted linear fit to the data (thick line: best fit, gray lines: ±1σ variation); x axis error bars shown for each sample.

sides of the Motagua Fault (Figure 7A) [*Harlow et al.*, 2004; *Ratschbacher et al.*, 2009]. The Chuacús complex was affected by a single event of rapid cooling during Late-Cretaceous time when it passed the ~550°C (hornblende ^{40}Ar-^{39}Ar closure temperature) and 275–350°C (biotite and muscovite ^{40}Ar-^{39}Ar closure temperatures) isotherms between 75 and 65 Ma. South of the Motagua Fault, the pattern of ^{40}Ar-^{39}Ar ages is more complex. The western part of Las Ovejas records cooling events at ~165 and ~125 Ma, including localized Middle Jurassic to Early Cretaceous reheating [*Ratschbacher et al.*, 2009] followed by Early Cretaceous retrogression during blueschist-facies metamorphism of ophiolitic rocks [*Brueckner et al.*, 2009]. The ^{40}Ar-^{39}Ar ages decrease abruptly toward the east, recording cooling events at around 40 and 20 Ma (Figure 7A). *Ratschbacher et al.* [2009] proposed that the ages around 40 Ma record the deformation and rapid cooling of the Las Ovejas complex, and that ages around 20 Ma could reflect a slower cooling phase or mineral crystallization below the closure temperature for Ar diffusion during a deformation event; clear synkinematic mineral growth supports the latter [*Ratschbacher et al.*, 2009]. Notwithstanding this lateral variability of ^{40}Ar-^{39}Ar ages along the Las Ovejas complex, the most striking, first-order pattern revealed by ^{40}Ar-^{39}Ar geochronology is a clear temporal asymmetry of the final cooling events across the Motagua Fault, with the Chuacús complex cooling 40 Ma earlier than the Las Ovejas complex (Figures 7A and 8A) [*Ratschbacher et al.*, 2009].

[25] Lower-temperature cooling is tracked by apatite fission track (AFT) ages that show a similar age jump across the Motagua Fault, with ages ranging from 55 to 18 Ma in the Chuacús complex, and from 24 to 7 Ma in the Las Ovejas complex (Figure 7C) [*Ratschbacher et al.*, 2009]. A cross-sectional representation of AFT ages (Figure 8C) shows that this difference cannot be attributed to differences in the elevation at which the samples were collected, but is clearly associated with the Motagua Fault. North of the fault, AFT ages suggest slower cooling but do not exhibit any clear trend with elevation; south of the fault, AFT ages show a better correlation with elevation

but also tend to be younger near the Motagua Fault (Figure 8C). The apparent tilt of AFT ages along the northern border of the Chortís block suggests a north-south lateral gradient in cooling evolution.

3.2. ZHe Analyses

[26] Samples for (U-Th)/He on zircon (ZHe) dating were collected along steep profiles on both sides of the lower Motagua valley. Estimated closure temperatures for the ZHe system vary slightly depending on grain size and rate of cooling. Diffusion parameters have been experimentally determined for zircon by *Reiners et al.* [2004] and yield a nominal closure temperature ranging from ~170 to 190°C, and a helium partial retention zone spanning a temperature range of 120 –180°C [*Tagami et al.*, 2003]. The ZHe thermochronometer has a closure temperature that bridges the gap between the ^{40}Ar-^{39}Ar and AFT thermochronometers [*Reiners*, 2005].

[27] Fifteen samples were analyzed to construct two age-elevation profiles on both sides of the Motagua valley (Figure 7B). The samples were collected below the upland relict surfaces approximately every ~100 m along the profiles, wherever possible. The northern profile (San Lorenzo) is composed of nine samples collected between 400 and 2300 m along a roughly north-south transect within the Chuacús complex. The southern profile (Chiquimula) is composed of four samples collected up the southern flank of the Motagua valley, between 200 and 1600 m within the Las Ovejas complex. The strong chemical alteration and small size of the zircons strongly limited the analyzable samples along this transect. In addition, two isolated samples have been collected in the western Chuacús complex and one north of the Polochic Fault.

[28] Mineral separation was performed following standard crushing, sieving, magnetic, and density separation procedures. Grains were hand-picked in the 80 to 200 μm fraction to select idiomorphic and inclusion-free specimens. The majority of (U-Th)/He analyses were performed at the ETH Zurich, and a subset was analyzed at the University of Arizona, following the method described by *Reiners et al.* [2004] in both laboratories. The abundance of He in each crystal was measured by laser mass spectrometry. The concentrations of U and Th were measured by isotope dilution. An α-ejection correction (Ft) was applied to each crystal to derive a corrected (U-Th)/He age [*Reiners*, 2005].

3.3. ZHe Results

[29] Table 2 displays the geographic coordinate, ZHe ages, and 1-sigma errors for all dated zircon grains. The reproducibility of ZHe ages is good, with an average 1-sigma error of about 8%. As in the case of the ^{40}Ar-^{39}Ar and AFT ages, the ZHe ages show a first-order discontinuity across the Motagua Fault: with ages between 55 and 30 Ma, cooling of the Chuacús complex is substantially older than cooling of the Las Ovejas complex (18–10 Ma; Figures 7B and 8B). Along the San Lorenzo profile, to the north of the Motagua Fault, ZHe ages range from 30.2 ± 1.1 Ma to 47.4 ± 2.3 Ma, following a very good linear trend of increasing ages with elevation ($R^2 = 0.85$; Figure 9) with a slope of 106 m/Ma (93–126 m /Ma with 95% confidence). The Las Ovejas ZHe ages range from 10.9 ± 1.9 Ma to 18.3 ± 4.0 Ma and correlate

positively with elevation ($R^2 = 0.99$) with a slope of 157 m/Ma (91–567 m /Ma with 95% confidence). Both ZHe age-elevation relationships have similar slopes, with a 20 Ma offset. Further north, the crossing of the Baja Verapaz shear zone and of the Polochic Fault is not marked by any substantial change in exhumation history, with ZHe ages of 55.1 ± 12.8 Ma beyond the Polochic Fault, which is not significantly older than those of the Chuacús complex (Figure 7B).

5. Discussion

5.1. Origin of the Thermochronologic Asymmetry Across the Motagua Fault

[30] Variability of the thermochronological record is classically interpreted to record variability of denudation patterns. After testing this hypothesis, we investigate whether the persistence of contrasted geothermal gradients that were transported and juxtaposed across the Motagua strike-slip Fault could explain the observed contrast in thermochronologic record.

5.1.1. Hypothesis 1: Asymmetry of the Denudation

[31] Here we test whether younger thermochronological ages south of the Motagua Fault record higher denudation in the Chortís block. Similar slopes in ZHe age-elevation relationships of ~110–150 m /Ma on both sides of the fault show that denudation rates were similar during the time-lapse recorded by ZHe ages (i.e., ~30–45 Ma north and ~10–20 Ma south of the fault). Consequently, the only way to reconcile the data is to allow a post-30 Ma decrease in denudation rate north of the fault and/or a post-10 Ma increase in denudation rate south of the fault.

[32] The evolution of topography and deformation across the Motagua Fault contradicts the idea of faster denudation of the southern block in the Miocene. The surface generally stands at a lower elevation than the Chuacús complex and has been experiencing stretching and localized subsidence since the late Miocene (~10.5 Ma) [Dengo et al., 1970; Rogers et al., 2002; Jordan et al., 2007]. Furthermore, the preservation and incision of low-relief surfaces of mid- to late Miocene age on both sides of the fault suggest a similar Miocene geomorphic and denudational evolution across the fault and do not support an asymmetry of Miocene denudation rates. Moreover, the low denudation rate of ~150 m/Ma of the Las Ovejas complex is confirmed by K-Ar ages and barometric data in the composite Chiquimula batholith (Figure 5) [Ratschbacher et al., 2009]. This study indicates that emplacement of the latest-stage magma occurred ~20 Ma at a depth of 3.0 to 5.0 km, implying an integrated denudation rate of 150–225 m /Ma over the last 20 Ma to bring these rocks to the surface, with no specific increase of exhumation rate after 10 Ma. Finally, the preservation of ^{40}Ar/^{39}Ar ages at ~ 110–120 Ma in the western Las Ovejas complex (Figure 7) [Brueckner et al., 2009] implies a limited thickness of total denudation south of the Motagua Fault. Consequently, all available geological, geomorphological, and thermochronological data testify against a significant asymmetry in denudation rates across the Motagua Fault.

5.1.2. Hypothesis 2: Asymmetry of the Geothermal Gradient

[33] The compilation of magmatic, volcanic, and heat flow data supports an asymmetric evolution of the thermal setting across the fault; the large-scale strike-slip displacement that has recently juxtaposed the cold Maya block to the north against the hot, arc-derived, Chortís block to the south, has generated this spatial asymmetry. Numerical simulations show that a persistent asymmetry in thermal input can account for a thermochronologic asymmetry. In order to quantitatively test this second hypothesis, we compare observed white mica ^{40}Ar-^{39}Ar, ZHe, and AFT cooling ages with synthetic thermochronologic ages obtained from our modeling results (modified version of Pecube). The model is constrained with available thermal, geological, and geomorphological data.

[34] Like in the previous models, this model starts at 85 Ma with a thermal gradient of 20°C/km in the Maya block ($Ha = 0 \, \mu W \, m^{-3}$) and 40°C/km in the Chortís block ($Ha = 2.9 \, \mu W \, m^{-3}$). These values correspond to the present-day thermal setting derived from heat flow data. Consequently, we assume a persistent and stable geothermal asymmetry. All other model parameters are equal in the two blocks. A uniform and steady vertical rock uplift velocity is imposed. The model starts with a flat topography that simulates the initial, low-relief surface and evolves after 10 My toward a synthetic topography with a 30 km wavelength and 2 km amplitude, simulating the Late Miocene incision of the Motagua valley.

[35] The two sides of the Motagua Fault are simulated separately to avoid lateral heat transfer across the Motagua Fault. Numerical simulations show that lateral heat transfer across the fault should produce a progressive age transition across a strike-slip fault (Figure 4). This is not the case with the three thermochronometers (^{40}Ar-^{39}Ar, ZHe, and AFT) used here, suggesting that lateral heat transfer and thus contact between two different thermal blocks is more recent than the thermochronologic record.

[36] Some recent thermochronologic studies have used Pecube coupled to the Neighborhood Algorithm to invert thermochronologic ages and extract relevant values for model parameters [e.g., Herman et al., 2010; Valla et al., 2010], but a pertinent inversion of thermochronologic data sets requires a numerical model reproducing all of the active and significant thermal processes in the defined study area [van der Beek et al., 2010]. Here we consider this 2D thermo-kinematic model as a simplification of the complex thermo-tectonic evolution of the MPFZ. Our goal is to evaluate the impact of the persistent geothermal asymmetry on the thermochronology across the Motagua Fault and not to reproduce the entire complexity. Limitations of the model are fully discussed in the next section.

[37] The best fit values to actual data are obtained for a steady vertical rock uplift of 170 m/Ma (Figure 10). In first order, the fit is very good overall, demonstrating that our model satisfactorily explains the data set. We show here that this slow and steady denudation rate explains quite well both cooling of the Chuacús complex since ~70 Ma (with 20°C/km geotherm) and cooling of the Las Ovejas complex (with 40°C/km geotherm) since ~35 Ma. A denudation rate of 170 m/Ma is compatible with the denudation rates estimated from ZHe age-elevation relationships, which are 110 and ~160 m/Ma for the Chuacús and Las Ovejas complexes, respectively, and consistent with the integrated 150–225 m /Ma denudation rates since 20 Ma in the Chortís block derived from the depth of emplacement of the Chiquimula batholith.
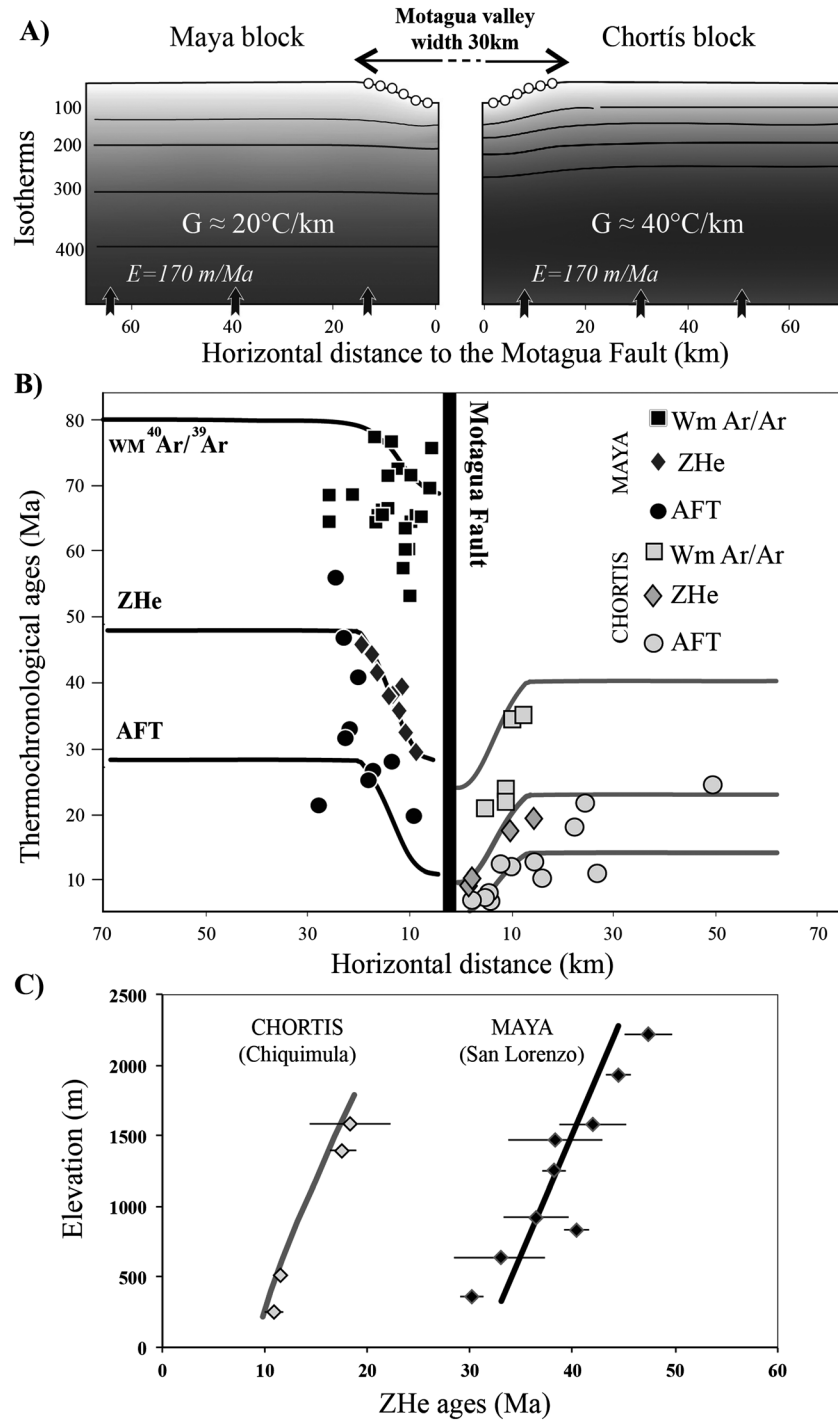
Figure 10. Thermal structure, thermochronology cross section, and age-elevation relationships plot comparing synthetic and observed thermochronologic ages for the Maya and Chortís blocks. Observed thermochronologic ages (white mica ^{40}Ar-^{39}Ar, ZHe, and AFT ages) and synthetic ages derived from modeling (solid lines) are projected along their horizontal distance from the Motagua Fault. See text for detailed description of the model setting (section 5.1.2.).

[38] The long-term spatial variability in thermal structure can strongly impact the thermochronological record. Numerical simulation of a persistent geotherm difference between two tectonic blocks sliding along a strike-slip fault demonstrates that this juxtaposition of blocks is sufficient to reproduce satisfactorily the observed asymmetry without calling for differences in denudation rates.

5.2. Limitations of the Thermal Model

[39] Some residual misfit between observed and synthetic data indicates that our model does not fully reproduce the cooling and tectonic evolution of the MPFZ. First, a steady denudation rate since 85 Ma is at odds with the two-stage exhumation of the Chuacús rocks since the Late Cretaceous [*Ratschbacher et al.*, 2009]. The simulation of middle and
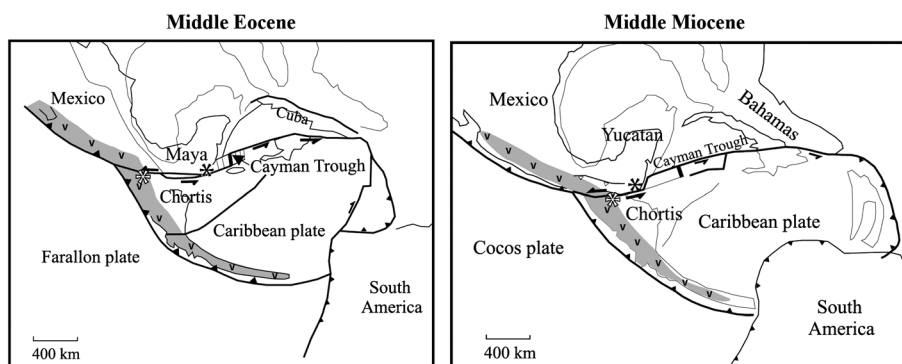
Figure 11. Paleogeography and tectonics of the Caribbean plate at A) the Eocene and B) Middle Miocene from *Morán-Zenteno et al.* [2009], *Mann* [2007], and *Ratschbacher et al.* [2009]. Black and white stars show locations of San Lorenzo (Chuacus complex) and Chiquimula (Las Ovejas complex) profiles, respectively.

high-temperature thermochronometers such as [40]Ar-[39]Ar ages on K-feldspar, biotite, or hornblende would be necessary to reproduce the Late Cretaceous rapid cooling event. Second, in addition to this major tectonic unroofing, Chuacùs rocks are locally intruded at ~76–66 Ma by upper-crustal pegmatites [*Ratschbacher et al.*, 2009; *Martens et al.*, 2012], their emplacements are not simulated and could have locally perturbed the thermal structure. Third, the model only calculates thermochronological ages by rock cooling and not by syn-deformational mineral crystallization below the closure temperature of Ar diffusion. Then, modeling does not reproduce old [40]Ar/[39]Ar ages at ~110–120 Ma in the western Las Ovejas complex (Figure 7) [*Brueckner et al.*, 2009]. As discussed previously, the conservation of these Early Cretaceous cooling ages implies a limited total denudation south of the Motagua Fault, but the origin of this lateral variability in the Las Ovejas complex is difficult to evaluate in the present state of knowledge of the Tertiary deformation and magmatic evolution of the Las Ovejas complex. Finally, we do not simulate the east-west extension of the Chortís block since late Miocene time (by ~10.5 Ma) [*Dengo et al.*, 1970; *Rogers et al.*, 2002], which has probably impacted the thermochronological data set.

[40] In summary, the complexity of the tectonic evolution of the MPFZ is not fully reproduced by our modeling, but the variability of the thermal structure either sides of the Motagua Fault clearly appears as the first-order process controlling white mica [40]Ar-[39]Ar, ZHe, and AFT ages. More generally, we show here that thermochronological data are not a direct measurement of denudation patterns, but rather than function of both denudation processes through tectonic and erosion processes, and thermal processes such geothermal difference across a strike-slip fault.

5.3. Origin of Persistent Difference in Geothermal Gradients Across the Motagua Fault

[41] The Chortís block is believed to have been originally located along the Pacific margin of Mexico [*Karig*, 1978; *Gose*, 1985; *Pindell et al.*, 1988; *Ross and Scotese*, 1988; *Schaaf et al.*, 1995; *Mann*, 2007]. Indeed, high shear stress across the Caribbean-North American plate boundary during the Eocene triggered breakaway of the Chortís Block from

southern Mexico, coeval with initiation of the Cayman trough pull-apart basin. This sinistral break away started in the Xolapa complex (Figure 1A) that had been an arc at least since Late Cretaceous and thus was thermally weakened. This terrane started drifting eastward in the wake of the Caribbean plate and migrated along the plate margin, over the subducting slab, remaining in an arc position between the continental interior of North America and the subduction zone (Figure 11) [*Mann*, 2007; *Ratschbacher et al.*, 2009]. From a thermal point of view, the Chortís block has stayed in an arc position and thus continuously intruded by a large amount of magma, which explains the persistence of a high geothermal gradient since the Eocene.

[42] In contrast, the northern side of the Motagua valley, the Maya block, has remained in a back-arc position for the last 65 Ma, far from any arc activity. Since the Middle Miocene, displacement of the Chortís block along the southwestern margin of the North America plate brought the Maya block closer to the subduction (Figure 11) [e.g., *Pindell and Kennan*, 2009], but igneous activity along the Sierra de Chiapas has remained probably too sparse to significantly increase the crustal geothermal gradient (Figure 1B). The flat slab geometry of the subducted Cocos plate beneath the Sierra de Chiapas has induced a 450 km long volcanic gap between the eastern end of the Trans-Mexican Volcanic Belt to the northwest and the northwestern end of the narrow Central American Volcanic Arc to the southeast [*Manea and Manea*, 2006].

[43] Numerical simulations show that the lateral transport of two tectonic blocks with different geotherm should produce lateral heat transfer across the fault and a progressive age transition across the Motagua Fault. This is not the case with the three thermochronometers ([40]Ar-[39]Ar, ZHe, and AFT) used here, suggesting that lateral heat transfer is likely more recent than the thermochronologic record. Heat transfer would have to occur after 7–10 Ma in the Chortís block and after 20–25 Ma in the Maya block. Before the Middle Miocene, the northeastern side of Chortís (northeast of the Las Ovejas complex) was also a magmatic arc [*Solari et al.*, 2007; *Ratschbacher et al.*, 2009; *Torres de León et al.*, 2012] with likely hot geothermal conditions, a possible explanation for the lack of heat exchange. Lower-temperature thermochronometers, such as apatite (U-Th)/He, would be

necessary to detect and date the onset of heat transfer across the Motagua Fault and therefore understand the initiation of the modern situation with a Motagua Fault acting as a thermal boundary.

6. Conclusions

[44] Published ^{40}Ar-^{39}Ar and AFT ages combined with new ZHe age-elevation relations show a pronounced cooling age discontinuity across the Motagua Fault. The present-day surface heat flow, slopes of the age-elevation relationships, geomorphologic features, and thermo-kinematic modeling results all suggest similar denudation rates across the fault since the Oligocene. A period of moderate denudation (~170 m/Ma) allowed for the formation of low-relief landscapes on both blocks prior to the inception of surface uplift since the Middle-Upper Miocene. The contrasted age patterns across the fault and the ZHe age-elevation relations are better explained by a persistent difference in geothermal gradient, the Motagua Fault now juxtaposing the cold Maya block and the hot Chortís block. This work highlights the importance of considering lateral variations of the geotherm, and not only differential denudation mechanisms, when interpreting age patterns and age-elevation variability across strike-slip faults.

References

Anderson, T. H., R. J. Erdlac Jr., and M. A. Sandstrom (1985), Late-Cretaceous allochthons and post-Cretaceous strike-slip displacement along the Cuilco-Chixoy-Polochic fault, Guatemala, *Tectonics*, *4*, 453–475, doi:10.1029/TC004i005p00453.

Authemayou, C., G. Brocard, C. Teyssier, T. Simon-Labric, A. Guttiérrez, E. N. Chiquín, and S. Morán (2011), Caribbean-North America-Cocos triple junction and the dynamics of the Polochic-Motagua fault system: a zipper model, *Tectonics*, *30*, TC3010, doi:10.1029/2010TC002814.

Authemayou, C., L. Bellia, G. Brocard, C. Teyssier, B. Suski, B. Cosenza, S. Moran-Ical, C. W. Gonzalez-Véliz, M. A. Aguilar-Hengstenberg, and K. Hollinger (2012), Quaternary seismo tectonic activity of the Polochic Fault, Guatemala. *J. Geophys. Res.*, *117*, B07403, doi:10.1029/2012JB009444.

Beccaluva, L., S. Bellia, M. Coltorti, G. Dengo, G. Giunta, J. Mendez, J. Romero, S. Rotolo, and F. Siena (1995), The northwestern border of the Caribean Plate in Guatemala: new geological and petrological data on the Motagua ophiolitic belt, *Ofioliti*, *20*(1), 1–15.

van der Beek, P. A., P. G. Valla, F. Herman, J. Braun, C. Persano, K. J. Dobson, and E. Labrin (2010), Inversion of thermochronological age-elevation profiles to extract independent estimates of denudation and relief history– II: Application to the French Western Alps, *Earth Planet. Sci. Lett.*, *296*, 9–22, doi:10.1016/j.epsl.2010.04.032.

Bermudez, M. A., P. A. van der Beek, and M. Bernet (2011), Asynchronous Mio-Pliocene exhum-ation of the central Venezuelan Andes, *Geology*, *39*, 139–142, doi:10.1130/G31582.1.

Bigot-Cornier, F., C. Basile, G. Poupeau, J. P. Bouillin, and E. Labrin (2005), Denudation of the Côte d'Ivoire-Ghana transform continental margin from apatite fission tracks, *Terra Nova*, *17*, 189–195, doi:10.1111/j.1365-3121.2005.00605.x.

Blackwell, D. D., and M. Richards (2004), Geothermal Map of North America, *American Assoc. Petroleum Geologist* (*AAPG*), 1 sheet, scale 1:6,500,000.

Bolge, L. L., M. J. Carr, K. I. Milidakis, F. N. Lindsay, and M. D. Feigenson (2009), Correlating geochemistry, tectonics, and volcanic volume along the Central American volca- nic front, *Geochem. Geophys. Geosyst.*, *10*, Q12S18, doi:10.1029/2009GC002704.

Bouillin, J. P., G. Poupeau, E. Labrin, C. Basile, N. Sabil, J. Mascle, F. Gillot, and L. Riou (1997), Fission track study: heating and denudation of marginal ridge of the Ivory Coast– Ghana transform margin, *Geol. Mar. Lett.*, *17*, 55–61.

Braun, J. (2002), Quantifying the effect of recent relief changes on age elevation relationships, *Earth Planet. Sci. Lett.*, *200*, 331–343, doi:10.1016/S0012-821X(02)00638-6.

Braun, J., P. van der Beek, and G. Batt (2006), *Quantitative Thermochronology: Numerical Methods for the Interpretation of Thermochronological Data*, 258 pp., Cambridge Univ. Press, New York, doi:10.1017/CBO9780511616433.

Braun, J., P. van der Beek, P. Valla, X. Robert, F. Herman, C. Glotzbach, V. Pedersen, C. Perry, T. Simon-Labric, and C. Prigent (2012), Quantifying rates of landscape evolution and tectonic processes by thermochronology and numerical modeling of crustal heat transport using PECUBE, *Tectonophysics*, *524–525*, 1–28, doi:10.1016/j.tecto.2011.12.035.

Brocard, G., C. Teyssier, W. J. Dunlap, C. Authemayou, T. Simon-Labric, L. Chiquín, A. Guttierrez, and S. Morán (2011), Reorganization of a deeply incised drainage: role of deformation, sedimentation and ground-water flow, *Basin Res.*, *23*, doi:10.1111/j.1365-2117.2011.00510.x.

Brueckner, H. K., H. G. Avé Lallemant, V. B. Sisson, G. E. Harlow, S. R. Hemming, U. Martens, T. Tsujimori, and S. S. Sorensen (2009), Metamorphic reworking of a high pressure–low temperature mélange along the Motagua fault, Guatemala: a record of Neocomian and Maastrichtian transpressional tectonics, *Earth Planet. Sci. Lett.*, *284*, 228–235, doi:10.1016/j.epsl.2009.04.032.

Burkart, B. (1978), Offset across the Polochic fault of Guatemala and Chiapas, Mexico, *Geology*, *6*, 328–332, doi:10.1130/0091-7613.

Burkart, B. (1983), Neogene North America–Caribbean plate boundary across northern Central America: Offset along the Polochic fault, *Tectonophysics*, *99*, 251–270, doi:10.1016/0040-1951(83)90107-5.

Burkart, B. (1994), Northern Central America, in *An Introduction: Jamaica, Caribbean Geology*, edited by S. Donavan and T. Jackson, pp. 265–284, UWI Publ. Assoc, Kingston, Jamaica.

Burkart, B., B. C. Deaton, and G. Moreno (1987), Tectonic wedges and offset Lamaride structures along the Polochic fault of Guatemala and Chiapas, Mexico: Reaffirmation of large Neogene displacement, *Tectonics*, *6*, 411–422, doi:10.1029/TC006i004p00411.

Carr, M. J., and R. E. Stoiber (1990), Volcanism, in *The Geology of North America: The Caribbean Region*, edited by G. Dengo and J. E. Case, 375–391, Geol. Soc. of Am, Boulder, Colo.

Carr, M. J., M. D. Feigenson, L. C. Patino, and J. A. Walker (2003), Volcanism and geochemistry in Central America: Progress and problems, in *Inside the Subduction Factory, Geophys. Monogr. Ser., vol. 138*, AGU, Washington, D. C., pp. 153–179 .

Clemons, R. E. (1966), Geology of the Chiquimula quadrangle, Guatemala, Central America. *PhD thesis*, *University of Texas*, Austin.

Cruz, L., A. Fayon, C. Teyssier, and J. Weber (2007), Exhumation and deformation processes in transpressional orogens: The Venezuelan Paria Peninsula, SE Caribbean- South American plate boundary, in *Exhumation Associated with Continental Strike-Slip Fault Systems: Geological Society of America Special Paper*, edited by A. B. Till, S. M. Roeske, J. C. Sample, and D. A. Foster, *434*, 149–165, doi:10.1130/2007.2434(08).

Currie, C. A., K. Wang, R. D. Hyndman, and J. He (2004), The thermal effects of steady-state slab-driven mantle flow above a subducting plate: The Cascadia subduction zone and backarc, *Earth Planet. Sci. Lett.*, *223*, 35–48, doi:10.1016/j.epsl.2004.04.020.

Deaton, B. C., and B. Burkart (1984), Time of sinistral slip along the Polochic fault of Guatemala, *Tectonophysics*, *102*, 297–313.

DeMets, C., P. Jansma, G. S. Mattioli, T. H. Dixon, F. Farina, R. Bilham, E. Calais, and P. Mann (2000), GPS constraints on Caribbean-North America plate motion, *Geophys. Res. Lett.*, *27*, 437–440.

Dengo, G., O. Bohnenberger, and S. Bonis (1970), Tectonics and volcanism along the Pacific Marginal Zone of Central America, *Int. J. Earth Sci.*, *59*, 1215–3262.

Donnelly, T. W., G. S. Horne, R. C. Finch, and E. Lopez-Ramos (1990), Northern Central America; the Maya and Chortís blocks, in *The Geology of North America*, vol. H, The Caribbean Region, edited by G. Dengo and J. E. Case, 37–76, Geol. Soc. of Am., Boulder, Colo.

Donnelly, T. W., W. E. Bocs, S. Reeves, B. Burkart, D. Lawrence, D. Schwartz, W. Newcomb, W. Montgomery, P. Roper, and S. Prucha (1974), *Geological map of Guatemala, sheet of the central Motagua River*, Inst. Geogr. Nac, Guatemala City, Guatemala.

Donnelly, T. W., G. S. Horne, R. C. Finch, and E. Lopez-Ramos (1990), Northern Central America; the Maya and Chortís blocks, in *The Geology of North America*, vol. H, The Caribbean Region, edited by G. Dengo and J. E. Case, pp. 37–76, Geol. Soc. Am., Boulder, Colo.

Fitzgerald, P. G., R. B. Sorkhabi, T. F. Redfield, and E. Stump (1995), Uplift and denudation of the central Alaska Range: A case study in the use of apatite fission track thermochronology to determine absolute uplift parameters, *J. Geophys. Res.*, *100*, 20175–20191.

García-Palomo, A., J. L. Macías, and J. M. Espíndola (2004), Strike-slip faults and K-alkaline volcanism at El Chichon volcano, southeastern Mexico, *J. Volcanol. Geotherm. Res.*, 136, 247–268, doi:10.1016/j.jvolgeores.2004.04.001.

Gose, W. A. (1985), Paleomagnetic results from Honduras and their bearing on Caribbean tectonics, *Tectonics*, 4, 565–585.

Guzmán-Speziale, M. (2010), Beyond the Motagua and Polochic faults: Active strike-slip faulting along the western North America-Caribbean plate boundary zone, *Tectonophysics*, 496, 17–27, doi:10.1016/j.tecto.2010.10.002.

Hames, W. E., and S. A. Bowring (1994), An empirical evaluation of the argon diffusion geometry in muscovite, *Earth Planet. Sci. Lett.*, 124, 161–169.

Harlow, G. E., S. R. Hemming, H. G. Ave Lallement, V. B. Sisson, and S. S. Sorensen (2004), Two high-pressure low temperature serpentinite-matrix melange belts, Motagua fault zone, Guatemala: a record of Aptian and Maastrichtian collisions, *Geology*, 32, 17–20, doi:10.1130/G19990.1.

Herman, F., et al. (2010), Exhumation, crustal deformation, and thermal structure of the Nepal Himalaya derived from the inversion of thermochronological and thermobarometric data and modeling of the topography, *J. Geophys. Res.*, 115, B06407, doi:10.1029/2008JB006126.

Holcombe, T. L., J. W. Ladd, G. Westbrook, N. T. Edgar, and C. L. Bowland (1990), Caribbean marine geology; ridges and basins of the plate interior, in *The Geology of North America*, vol. H, The Caribbean Region, edited by G. Dengo and J. E. Case, 231–260, Geol. Soc. of Am., Boulder, Colo.

Horne, G. S., G. S. Clark, and P. Pushkar (1976), Pre-Cretaceous rocks of northwestern Honduras: Basement terrane in Sierra de Omoa, *Am. Assoc. Pet. Geol. Bull.*, 60, 566–583.

Hourigan, J. K., P. W. Reiners, and M. T. Brandon (2005), U-Th zonation-dependent alpha-ejection in (U-Th)/He chronometry, *Geochim. Cosmochim. Acta*, 69, 3349–3365, doi:10.1016/j.gca.2005.01.024.

Jordan, B. R., H. Sigurdsson, S. Carey, S. Lundin, R. D. Rogers, B. Singer, and M. Barquero-Molina (2007), Petrogenesis of Central American Tertiary ignimbrites and associated Caribbean Sea tephra, in *Geologic and Tectonic Development of the Caribbean Plate Boundary in Northern Central America*, edited by P. Mann, *Spec. Pap. Geol. Soc. Am.*, 428, 151–178, doi:10.1130/2007.2428(07).

Karig, D. E. (1978), Late Cenozoic Subduction and Continental Margin Truncation Along the Northern Middle America Trench, *Geol. Soc. Am. Bull.*, 89, 265–276.

Kesler, S. E. (1970), Nature of ancestral orogenic zone in nuclear Central America, *AAPG Bull.*, 55, 2116–2129.

Kesler, S. E., W. L. Josey, and E. M. Collins (1970), Basement rocks of western nuclear Central America: The western Chuacús Group, Guatemala, *Geol. Soc. Am. Bull.*, 81, 3307–3322, doi:10.1130/0016-7606.

Kozuch, M. (1991), Mapa Geológica de Honduras: Tegucigalpa, Honduras, *Instituto Geográfi co Nacional*, 3 sheets, scale 1:500,000.

Le Pichon, X., C. Kreemer, and N. Chamot-Rooke (2005), Asymmetry in elastic properties and the evolution of large continental strike-slip faults, *J. Geophys. Res.*, 110, B03405, doi:10.1029/2004JB003343.

Leroy, S., A. Mauffret, P. Patriat, and B. Mercier de Lepinay (2000), An alternative interpretation of the Cayman Trough evolution from a re-identification of magnetic anomalies, *Geophys. J. Int.*, 141, 539–557.

Lyon-Caen, H., et al. (2006), Kinematics of the North American-Caribbean-Cocos plates in Central America from new GPS measurements across the Polochic-Motagua fault system, *Geophys. Res. Lett.*, 33, L19309, doi:10.1029/2006GL027694.

Macdonald, K. C., and T. L. Holcombe (1978), Inversion of magnetic anomalies and sea- floor spreading in the Cayman Trough, *Earth Planet. Sci. Lett.*, 40, 407–414.

Manea, V. C., and M. Manea (2006), The origin of modern Chiapanecan volcanic arc in Southern Mexico inferred from thermal models. GSA Special Paper 412: Natural Hazards in Central America, 27–38, doi:10.1130/2006.2412(02).

Mann, P. (2007), Overview of the tectonic history of northern Central America, in *Geologic and tectonic development of the Caribbean plate boundary in northern Central America*, *Geol. Soc. of Am.*, vol. 428, edited by P. Mann, pp. 1–19, doi:10.1130/2007.2428(01).

Martens, U., H. K. Brueckner, C. G. Mattinson, J. G. Liou, and J. Wooden (2012), Timing of eclogite-facies metamorphism of the Chuacús Complex, central Guatemala: Record of Late Cretaceous continental subduction of North America's sialic basement, *Lithos*, 146–147, 1–10, doi:10.1016/j.lithos.2012.04.021.

McBirney, A. R. (1963), Geology of a part of the Central Guatemalan Cordillera, University of California Publications in Geological Sciences, 38, 177–242.

Meert, J. G., and D. L. Smith (1991), Heat flow at the Platanares, Honduras, geothermal site, in *Honduras- A Geothermal Investigation*, edited by F. Goff, *J. Volcanol. Geotherm. Res.*, 45, 91–99, Elsevier Science Publishers B.V., Amsterdam.

Mora, J. C., M. Jaimes-Viera, H. Garduno-Monroy, P. Layer, V. Pompa-Mera, and M. Godinez (2007), Geology and geochemistry characteristics of the Chiapanecan volcanic arc (central area), Chiapas Mexico, *J. Volcanol. Geotherm. Res.*, 162, 43–72, doi:10.1016/j.jvolgeores.2006.12.009.

Morán-Zenteno, D. J., D. J. Keppie, B. Martiny, and E. González-Torres (2009), Reassessment of the Paleogene position of the Chortís block relative to southern Mexico: Hierarchical ranking of data and features, *Rev. Mex. Cienc. Geol.*, 26, 177–188.

Muehlberger, W. R., and A. W. Ritchie (1975), Caribbean-Americas plate boundary in Guatemala and southern Mexico as seen on Skylab IV orbital photography, *Geology*, 3, 232–235, doi:10.1130/0091-7613.

Ortega-Gutiérrez, F., L. A. Solari, J. Solé, U. Martens, A. Gomez-Tuenam, S. Moran-Ical, M. Reyes-Salas, and C. Ortega-Obregon (2004), Polyphase, high-temperature eclogite-facies metamorphism in the Chuacús complex, central Guatemala: Petrology, geochronology and tectonic implications, *International Geology Review*, 46, 445–470, doi:10.2747/0020-6814.46.5.445.

Ortega-Gutiérrez, F., L. Solari, C. Ortega-Obregón, M. Elías-Herrera, U. Martens, S. Moral-Icál, M. Chiquín, J. Duncan Keppie, R. Torres de León, and P. Schaaf (2007), The Maya-Chortis boundary: A tectonostratigraphic approach, *Int. Geol. Rev.*, 49, 996–1024, doi:10.2747/0020-6814.49.11.996.

Ortega-Obregon, C., L. A. Solari, J. D. Keppie, F. Ortega-Gutierrez, J. Solé, and S. Moran-Ical (2008), Middle-Late Ordovician magmatism and Late Cretaceous collision in the southern Maya block, Rabinal-Salamá area, central Guatemala: Implications for North America–Caribbean plate tectonics, *Geol. Soc. Am. Bull.*, 120, 556–570, doi:10.1130/B26238.1.

Pindell, J. L., L. Kennan (2009), Tectonic evolution of the Gulf of Mexico, Caribbean and Northern South America in the mantle reference frame: An update, in *The Origin and Evolution of the Caribbean Plate*: *Geol. Soc. Spec. Publ.*, vol. 328, edited by K. H. James, M. A. Lorente, and J. L. Pindell, pp. 1–55, doi:10.1144/SP328.1.

Pindell, J. C., S. C. Cande, W. C. Pitman, D. B. Rowley, J. F. Dewey, J. Labrecque, and W. Haxby (1988), A plate kinematic framework for models of the Caribbean evolution, *Tectonophysics*, 155, 121–138.

Pindell, J., L. Kennan, W. V. Maresch, K. P. Stanek, G. Draper, and R. Higgs (2005), *Plate-kinematics and crustal dynamics of circum-Caribbean arc-continent interactions, and tectonic controls on basin development in Proto-Caribbean margins, Caribbean–South American Plate interactions, Venezuela, Geol. Soc. of Am.*, vol. 394, edited by H. G. Avé-Lallemant, and V. B. Sisson, pp. 7–52, doi:10.1130/2005.2394(01).

Plafker, G. (1976), Tectonic aspects of the Guatemala earthquake of 4 February 1976, *Science*, 93, 1201–1208.

Ratschbacher, L., et al. (2009), The north American–Caribbean plate boundary in Mexico-Guatemala-Honduras, in *The Origin and Evolution of the Caribbean Plate*, edited by K. H. James, M. A. Lorente, J. L. Pindell, *Geol. Soc. Spec. Publ.*, 328, pp. 219–293, doi:10.1144/SP328.11.

Reed, J. C., J. O. Wheeler, and B. E. Tucholke (2005), *Geologic map of North America: perspectives and explanation*, Geological Society of America, Decade of North American Geology, Boulder, CO.

Reiners, P. W. (2005), Zircon (U-Th)/He thermochronometry, *Rev Mineral Geochem*, 58(151), 179, doi:10.2138/rmg.2005.58.6.

Reiners, P. W., T. L. Spell, S. Nicolescu, and K. A. Zanetti (2004), Zircon (U-Th)/He thermochronology: He diffusion and comparisons with $^{40}Ar/^{39}Ar$ dating, *Geochim. Cosmochim. Acta*, 68, 1857–1887, doi:10.1016/j.gca.2003.10.021.

Ritchie, A. W. (1976), Jocotán Fault; possible western extension, Publicaciones Geológicas del ICAITI (Guatemala), 5, 52–55.

Rogers, R. D., and P. Mann (2007), Transtensional deformation of the western Caribbean– North America plate boundary zone, in *Geologic and Tectonic Development of the Caribbean Plate Boundary in Northern Central America*, *Geol. Soc. of Am.*, vol. 428, edited by P. Mann, doi:10.1130/2007.2428(02).

Rogers, R. D., H. Kàrason, and R. D. van der Hilst (2002), Epeirogenic uplift above a detached slab in northern Central America, *Geology*, 30, 1031–1034.

Rogers, R. D., P. Mann, and P. A. Emmet (2007), Tectonic terranes of the Chortis block based on integration of regional aeromagnetic and geologic data, in *Geologic and Tectonic Development of the Caribbean Plate in northern Central America*: *Geol. Soc. of Am.*, vol. 428, edited by P. Mann, 65–88, doi:10.1130/2007.2428(04).

Rosencrantz, E., M. I. Ross, and J. G. Sclater (1988), The age and spreading history of the Cayman Trough as determined from depth, heat flow, and magnetic anomalies, *J. Geophys. Res.*, 93, 2141–2157.

Ross, M., and C. R. Scotese (1988), A hierarchical tectonic model of the Gulf of Mexico and Caribbean region, *Tectonophysics*, 155, 139–168.

Sage, F., C. Basile, J. Mascle, B. Pontoise, and R. Whitmarsh (2000), Crustal structure of the continent-ocean transition off the Côte d'Ivoire-Ghana transform margin: implications for thermal exchanges across the paleo-transform boundary, *Geophys. J. Int.*, 143, 662–678.

Schaaf, P., D. Morán-Zenteno, M. Hernández-Bernal, G. Solís-Pichardo, G. Tolson, and H. Köhler (1995), Paleogene continental margin truncation in southwestern Mexico: geochronological evidence, *Tectonics*, *14*, 1339–1350.

Schwartz, D. P., L. S. Cluff, and T. W. Donnelly (1979), Quaternary faulting along the Caribbean-North America plate boundary in Central America, *Tectonophysics*, *52*, 431–445.

Sigurdsson, H., S. Kelley, R. M. Leckie, S. Carey, T. Bralower, J. King (2000), History of circum-Caribbean explosive volcanism: ^{40}Ar/^{39}Ar dating of tephra layers. In *Proc. ODP, Sci. Results*, 165, edited by R. M. Leckie, H. Sigurdsson, G. D. Acton, and G. Draper, p. 299–314, College Station, TX, Ocean Drilling Program, doi:10.2973/odp.proc.sr.165.021.2000

Solari, L. A., R. Torres de León, G. Hernández Pineda, J. Solé, G. Solís-Pichardo, and T. Hernández-Treviño (2007), Tectonic significance of Cretaceous–Tertiary magmatic and structural evolution of the northern margin of the Xolapa Complex, Tierra Colorada area, southern Mexico, *Geol. Soc. Am. Bull.*, *119*, 1265–1279, doi:10.1130/B26023.1.

Spotila, J. A., M. A. House, N. A. Niemi, R. C. Brady, M. Oskin, J. T. Buscher (2007), Patterns of bedrock uplift along the San Andreas fault and implications for mechanisms of transpression, in *Exhumation Associated with Continental Strike-Slip Fault Systems*, *Geol. Soc. of Am.*, 434, edited by A. B. Till, S. M. Roeske, J. C. Sample, and D. A. Foster, pp. 15–33, doi:10.1130/2007.2434(02).

Stephenson, J., K. Gallagher, and C. C. Holmes (2006), A Bayesian approach to calibrating apatite fission track annealing models for laboratory and geological timescales, *Geochim. Cosmochim. Acta*, *70*, 5183–5200, doi:10.1016/j.gca.2006.07.027.

Storti, F., R. E. Holosworth, and F. Salvini (2003), Intraplate strike-slip deformation belts, in *Intraplate Strike-slip Deformation Belts*, edited by F. Storti et al., *Geol. Soc. Spec. Publ.*, vol. 210, 1–14, doi:10.1144/GSL. SP.2003.210.01.01.

Sutter, J. F. (1979), Late Cretaceous collisional tectonics along the Motagua fault zone, Guatemala, *Geological Society of America, Abstracts with Programs*, *11*, 525–526.

Tagami, T., K. A. Farley, and D. F. Stockli (2003), Thermal sensitivities of zircon (U-Th)/He and fission-track systems, *Geochim. Cosmochim. Acta*, *67*(18), 466.

Torres de León, R., L. Solari, F. Ortega-Gutiérrez, and U. Martens (2012), The Chortís block–southwestern Mexico connections: U-Pb zircón

geochronology constraints, *Am. J. Sci.*, *312*, 288–313, doi:10.2475/03.2012.02.

Touloukian, Y. S., W. R. Judd, and R. F. Roy (1981), *Physical Properties of Rocks and Minerals, Data Series on Material Properties*, 1–2, McGraw-Hill, New York.

Umhoefer, P. J., D. L. Whitney, C. Teyssier, A. K. Fayon, G. Casale, and M. T. Heizler (2007), Yo-yo tectonics in a wrench zone, Central Anatolian fault zone, Turkey. In *Exhumation Associated with Continental Strike-Slip Fault Systems*, *Geological Society of America*, *Boulder. Special Paper*, *434*, 35–58, doi:10.1130/2007.2434(03).

Valla, P. G., F. Herman, P. A. van der Beek, and J. Braun (2010), Inversion of thermochronological age-elevation profiles to extract independent estimates of denudation and relief history - I: Theory and conceptual model, *Earth Planet. Sci. Lett.*, *295*, 511–522, doi:10.1016/j.epsl.2010.04.033.

Walker, J. A., B. S. Singer, B. R. Jicha, B. I. Cameron, M. J. Carr, and J. L. Olney (2011), Monogenetic, behind-the-front volcanism in southeastern Guatemala and western El Salvador: ^{40}Ar/^{39}Ar ages and tectonic implications, *Lithos*, *123*, 243–253, doi:10.1016/j.lithos.2010.09.016.

Wawrzyniec, T. (2005), A newly discovered, relic, transcurrent plate boundary—The Tonala shear zone and paleomagnetic evaluation of the western Maya block, SW Mexico, Paper 28–52005 presented at Salt Lake City Annual Meeting, *Geol. Soc. of Am.*, Salt Lake City, Utah.

Weber, B., A. Iriondo, W. Premo, L. Hecht, and P. Schaaf (2007), New insights into the history and origin of the southern Maya block, SE Mexico: U-Pb-SHRIMP zircon geochronology from metamorphic rocks of the Chiapas massif, *Int. J. Earth Sci.*, *96*, 253–269, doi:10.1007/s00531-006-0093-7.

White, R. A. (1984), Catalog of historic seismicity in the vicinity of the Chixoy-Polochic and Motagua Faults. Guatemala. *U.S. Geological Survey*, Open-File Report, 84–88.

White, R. A. (1985), The Guatemala earthquake of 1816 on the Chixoy-Polochic fault, *Bull. Seismol. Soc. Am.*, *75*, 455–473.

Williams, H., and A. R. McBirney (1969), *Volcanic History of Honduras*, University of California Publications, vol. *85*, pp. 1–70.

Witt, C., S. Brichau, and A. Carter (2012), New constraints on the origin of the Sierra Madre de Chiapas (south Mexico) from sediment provenance and apatite thermochronometry, *Tectonics*, *31*, TC6001, doi:10.1029/2012TC003141.